Low Temperature Physics/Fizika Nizkikh Temperatur, 2018, v. 44, No. 7, pp. 775–793

Bullets and droplets: Two-dimensional spin-wave solitons in modern magnonics

(Review Article)

O.R. Sulymenko and O.V. Prokopenko

Taras Shevchenko National University of Kyiv, *Kyiv 01601*, *Ukraine*
E-mail: olgasulymenko@gmail.com, oleksandr.prokopenko@gmail.com

V.S. Tyberkevych and A.N. Slavin

Oakland University, *Rochester MI 48309*, *USA*
E-mail: tyberkev@oakland.edu; slavin@oakland.edu

A.A. Serga

Technische Universität Kaiserslautern, *Kaiserslautern 67663*, *Germany*
E-mail: serga@physik.uni-kl.de

Received February 14, 2018, published online May 28, 2018

In this review we consider theoretical and experimental results related to the properties of two-dimensional spin-wave (SW) solitons, so-called SW bullets and SW droplets. Such nonlinear self-localized SW modes possess very interesting physical properties, and could have practical applications in modern and future magnonics and spintronics. The experimental and theoretical results presented in this review have undeniably proven the existence of SW bullets in magnetic films and confined magnetic nanostructures (magnetic nanocontacts), and have elucidated the essential distinctions between the properties of the one-dimensional nonlinear SW solitons, two-dimensional nonlinear SW bullets and linear spin wave packets, as well as the possibility of self-generation, parametrical excitation, and phase-conjugation of the SW bullets, similar to the case of the conventional linear spin waves. Also, in this review we presented experimental results demonstrating the nucleation, dynamics, and annihilation of two-dimensional strongly nonlinear SW "droplets" in spin-torque-driven magnetic nanocontacts. The properties of these exotic nonlinear objects are analyzed using recently developed theoretical models and illustrated by micromagnetic numerical simulations.

PACS: 75.30.Ds Spin waves;
85.75.–d Magnetoelectronics; spintronics: devices exploiting spin polarized transport or integrated magnetic fields;
72.25.–b Spin-polarized transport;
73.50.Jt Galvanomagnetic and other magnetotransport effects (including thermomagnetic effects).

Keywords: magnetic soliton, spin-wave bullet, spin-wave droplet.

Contents

Preface

This review paper describes magnetic bullets and droplets — novel types of two-dimensional spin-wave solitons, which are the objects of intensive study in modern magnonics, and are interesting for the emerging field of applied spintronics. The paper was purposely written for the special issue of the "Low Temperature Physics" devoted to the 90th jubilee of Professor Arnold M. Kosevich, who made a series of seminal theoretical contributions to the development of magnonics, spintronics and nonlinear theory of solids. The authors would like to express their deep respect and gratitude to Professor A.M. Kosevich, whose theoretical work laid the foundation for the modern nonlinear magnetization dynamics, and made possible the theoretical and experimental work that is reviewed in this paper.

1. Introduction

As the magnetism of solids has a purely quantum nature, considerable progress in understanding the dynamical properties of such systems occurred after the publication of the article [1] by L. Landau and E. Lifshitz, where a simple quasi-classical phenomenological theory of magnetic excitations in solids was proposed. A decade later, after E. Zavoisky [2] and J. Griffiths [3] independently discovered in experiment the phenomena of ferromagnetic resonance (FMR), the stage of active study of magnetic dynamics at microwave frequencies began. In particular, the theory of ferromagnetic and antiferromagnetic resonances was developed [4–6], the properties of spin waves in bulk magnetic samples and magnetic films were studied [7–10], and various microwave magnetic devices were developed and used for practical applications [6,11,12]. A natural step in the study of spin waves was the transition from the investigation of linear spin waves to nonlinear waves [8,9] and, in particular, to the study of magnetic solitons.

A solitary nonlinear spin waves possess many interesting and unusual properties. Although solitons are known in physics for more than 180 years [13], their active study began only in the last third of the twentieth century [14–16].

A significant contribution to the theoretical description of magnetic solitons was made by Professor A.M. Kosevich, who published several key papers [17–19] in this field, which were also summarized in several reviews [20–22] and books [23–25].

In this review, we consider theoretical and experimental results related to the excitation, propagation and practical application of two types of two-dimensional magnetic or spin-wave (SW) solitons: magnetic bullets and droplets. Both these types of nonlinear solitonic SW excitations are now considered as promising "working objects" in modern magnonics and spintronics, and could be used for the development of a new generation of microwave information processing devices.

The review consists of the introduction, three main sections and conclusions. Section 2 contains a brief description of the physics of magnetic solitons, methods of their analysis, and conditions of their existence. Section 3 presents some theoretical and experimental results on magnetic bullets in magnetic films and magnetic layered nanostructures. Section 4 presents the results on the properties of recently experimentally discovered magnetic droplets.

2. Spin-wave soliton modes in magnets

The traditional approach to the description of the magnetization dynamics in magnetic systems is the use of the modified Landau–Lifshitz–Gilbert equation [6,26]:

$$\frac{\partial \mathbf{M}}{\partial t} = \gamma\left[\mathbf{H}_{\text{eff}} \times \mathbf{M}\right] + \frac{\alpha_G}{M_S}\left[\mathbf{M} \times \frac{\partial \mathbf{M}}{\partial t}\right] + \mathbf{T}. \qquad (1)$$

Here the first term in the right-hand side of the equation describes the conservative motion of the magnetization vector $\mathbf{M}$ in the effective magnetic field $\mathbf{H}_{\text{eff}}$, the second term describes the magnetic damping in a system, and the last term $\mathbf{T}$ describes any possible additional external influences on the magnetization $\mathbf{M}$ dynamics, for instance, the influences caused by a bias spin-polarized (or pure spin) current; γ is the gyromagnetic ratio, α_G is the Gilbert damping constant and $M_S = |\mathbf{M}|$ is the saturation magnetization.

Following A.M. Kosevich [22], it is natural to identify any localized in space stable solution of dynamical equation (1) as a magnetic soliton. In this review, however, we will restrict ourselves only to the dynamic SW envelope solitons, which can be naturally described using the standard Hamiltonian SW formalism [8]. In the framework of this formalism, Eq. (1) can be reduced to the nonlinear Schrödinger (NLS) equation with phenomenologically added term describing the magnetic damping in the considered system. For two-dimensional SW envelope solitons this $(2+1)$-dimensional NLS equation is usually written in the following form [9,27,28]:

$$i\left(\frac{\partial U}{\partial t} + v_g \frac{\partial U}{\partial z}\right) + \frac{1}{2} D \frac{\partial^2 U}{\partial z^2} + S \frac{\partial^2 U}{\partial y^2} - N |U|^2 U + i\omega_r U = 0. \qquad (2)$$

Here $U \equiv U(y,z,t) = \Psi(y,z,t) \exp\left[i(\omega_0 t - k_{0z} z)\right]$ is the slowly varying envelope function of the SW packet, ω_0 and k_{0z} are the angular frequency and longitudinal wave number of the soliton at some selected working point $(\omega_0; k_{0z})$ in the SW spectra, $v_g = \partial\omega/\partial k_z$ is the group velocity, $D = \partial^2\omega/\partial k_z^2$ and $S = \partial\omega/\partial(k_y^2)$ are the dispersion and diffraction coefficients, $N = \partial\omega/\partial(|\Psi|^2)$ is the nonlinear coefficient, $\omega_r = \gamma\Delta H$ is the dissipation parameter proportional to the FMR half-linewidth ΔH, and $\omega(k_y, k_z, |\Psi|^2)$ is the nonlinear dispersion law of a spin wave propagating in the film.

Also, the self-excitation of two-dimensional SW solitons Eq. (1) can be described in the framework of general nonlinear auto-oscillator model developed by A.N. Slavin and V.S. Tiberkevich in the context of the SW generation by spin-polarized currents [26,29]:

$$\frac{\partial c}{\partial t} + i\omega(c)c + \Gamma_+ c - \Gamma_- c = 0. \qquad (3)$$

This approach turned out to be rather fruitful, and was successfully verified in many experiments [30–32]. Also, in recent years it was frequently used for the description of nanoscale magnetic oscillators, detectors and other devices [33–46].

In Eq. (3) $c \equiv c(\mathbf{r},t)$ is the dimensionless complex SW amplitude which has a meaning similar to that of the envelope function U in (2), $\omega(c)$ is the nonlinear angular frequency of the magnetic excitation (in case when this excitation is a nonlinear propagating wave — the expression $\omega(c)$ contains the information about the wave dispersion D and nonlinearity N), Γ_+ is the conventional SW damping rate proportional to the Gilbert damping parameter α_G, $\Gamma_- = \sigma I\,(1-|c|^2) f(\mathbf{r})$ is the "negative" damping rate caused by the spin-polarized or spin current I traversing the system, σ is the coefficient characterizing the spin-transfer torque (STT) [47,48], and the dimensionless scalar function $f(\mathbf{r})$ describes the spatial distribution of the current [26,29]. It is worth noting, that Eq. (3), when it is applied to a current-induced excitation of a propagating spin wave, can be reduced to a driven and damped version of the NLS equation (2), while in the case when both damping and bias current are absent ($\Gamma_+ = \Gamma_- = 0$) — it is reduced to the conservative version of the NLS equation [28].

The major condition for the soliton existence is the conservation of its integrals of motion, such as energy, angular momentum, number of magnons, etc. [22]. However, usually, the necessary conditions for the soliton existence are formulated in terms of balance between the influence of nonlinearity, dispersion, diffraction and dissipation of a studied medium on the soliton formation [49].

There are several different approaches to the classification of solitons. The first and most simple classification is based on the dimensionality of the considered physical problem and its solution. In the scope of this approach solitons can be qualified as quasi-one-dimensional, two-dimensional (mainly considered in this review) or three-dimensional.

Another classification is based on the concepts of dynamic and topological solitons. Dynamic solitons can evolve in time and are stabilized due to the conservation of their total energy, total SW angular momentum or other integrals of motion [22,28]. In particular, dynamic solitons in conservative systems with no positive or "negative" damping ($\Gamma_+ = \Gamma_- = 0$) can be stable only when their dispersion law is balanced by their nonlinearity (the Lighthill criterion $ND < 0$) [49]. If a small perturbation disturbs the integrals of the motion, then the conservative dynamic soliton vanishes (a transition to the magnetization ground state occurs), or it transforms to the dissipative dynamic soliton, which can exist in a dissipative system, and has the modified integrals of motion.

Another type of solitons are topological solitons; they were studied in details by A.M. Kosevich and his co-authors [19,20,22,24,25]. They are special solutions of the equation of magnetization dynamics (or equivalent equation (3)), which are generated by the structure of the equation itself, and related to the overall symmetry of the considered problem [22]. Topological solitons can be divided into two groups, according to the magnetization localization: if the magnetization distribution does not depend on the coordinates far from the soliton it is called localized soliton, otherwise it is called nonlocalized soliton [22].

In this review we will restrict our attention to only one type of solitons — to the quasi-one-dimensional and two-dimensional SW envelope solitons [50], which were first experimentally observed in yttrium–iron–garnet (YIG) films [51] just after its theoretical prediction [52] for magnetostatic spin waves [53]. Such solitons are, usually, described by the NLS Eq. (2), and can exist when the Lighthill criterion $ND < 0$ [49] is fulfilled, while their stability is limited by the criterion $SN > 0$ (when $SN < 0$ these solitons can split into solitons in the direction perpendicular to the direction of its propagation) [9,27].

SW envelope solitons has been studied since the 1990s, using experimental observation of nonlinear dipole-exchange spin waves, backward-volume spin waves and spin waves in other geometries in YIG films [54–58].

The theory of SW envelope solitons has been developed in [59–63], parametric interaction of SW solitons using electromagnetic pumping and wave front reversal of SW envelope solitons has been studied in [64,65], generation of magnetic solitons trains has been observed in [66,67], amplification and compression of SW envelope soliton has been observed in [68,69], while formation of SW envelope solitons in periodic magnetic film structures has been studied in [70]. The majority of the obtained results were summarized in the reviews [59,71] and books [9,27,72–74].

In this review we will discuss in detail two particular type of the two-dimensional SW envelope solitons that are non-propagating and that are excited in magnetic films and nanostructures either by an external microwave signal, or by a spin-polarized or pure spin current. These are the spin-wave bullets and spin-wave droplets.

Spin-wave bullets (SW bullet) are the two-dimensional SW soliton pulses strongly localized in space and time by self-focusing.

The existence of wave bullets, which are stabilized by the saturation of the nonlinearity at high wave amplitudes, has been suggested in optics ("light bullets") by Y. Silberberg [75]. Wave bullets have been observed for light waves

in nonlinear optics and for nonlinear Langmuir waves in a plasma [76]. In magnetism, the SW bullets were experimentally observed in [77], and, then, have been intensively studied in magnetic films and nanostructures.

The spin-wave droplets (SW droplets) are the dissipative or conservative magnetic solitons existing in a system with perpendicular magnetic anisotropy (PMA) due to a balance between their nonlinearity, dispersion, and positive and "negative" damping [78]. Although they were predicted and theoretically studied by B.A. Ivanov and A.M. Kosevich as early as in 1977 [17], the first experimental observation of these interesting nonlinear excitations was reported only in 2013 [79] when the technique of SW excitation using spin-polarized currents was sufficiently developed. Since their theoretical prediction, the SW droplet type of magnetic solitons have been primarily studied theoretically or numerically by M.A. Hoefer and others [80–85] until recently, when they became a subject of intent look of experimentalists.

3. Spin-wave bullets in magnetic films and nanostructures

3.1. Spin-wave bullets in continuous YIG films and film stripes

Nonlinear self-focusing of wave beams and pulses resulting in the formation of a bullet is an important and well-known phenomenon in physics [86], experimentally observed for light waves in nonlinear optics, and for nonlinear Langmuir waves in a plasma [76]. However, the first observation of spatiotemporal self-focusing of SW beam, and the formation of a SW bullet was done only at the end of twentieth century [77]. The experimental results (Figs. 1, 2) were obtained for dipolar spin waves in YIG films by means of a space- and time-resolved Brillouin light scattering (BLS) technique [71]. The authors of [77] demonstrated self-focusing of a moving SW pulse in two spatial dimensions, and formation of a strongly localized SW bullet, the collapse of which is stopped by dissipation.

It is important to note, that in YIG films the diffraction to dispersion ratio is much smaller than in optical fibers, which makes it possible to observe in magnetic films a simultaneous self-focusing of a propagating SW packet along the both in-plane directions (see Fig. 1). In particular, in the experiment [77] the SW bullets were formed as a result of a spatiotemporal self-focusing, similar to the self-focusing effect in optics [75], as the two-dimensional input SW packets were self-focused for both in-plane directions (y and z), while propagating along z direction. The self-focusing of dipolar SW bullets in YIG films was stabilized by dissipation, rather than by saturation of nonlinearity, in contrast with the light bullets described in [75].

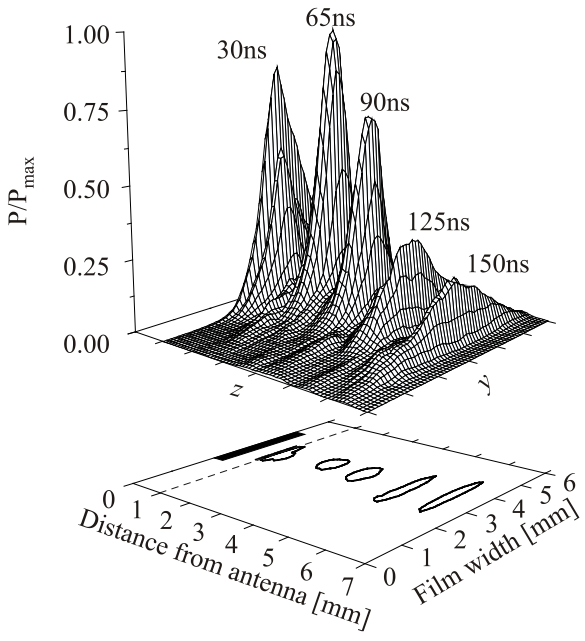

Fig. 1. Two-dimensional (y,z) distributions of normalized intensity in propagating dipolar SW packets, corresponding to five different values of the propagation (delay) time as indicated in the figure. The distributions were experimentally measured by space- and time-resolved BLS technique for $T = 29$ ns and $P_{in} = 460$ mW. The cross sections of the propagating wave packets taken at half-maximum power are shown on the (y,z) plane below. From [77].

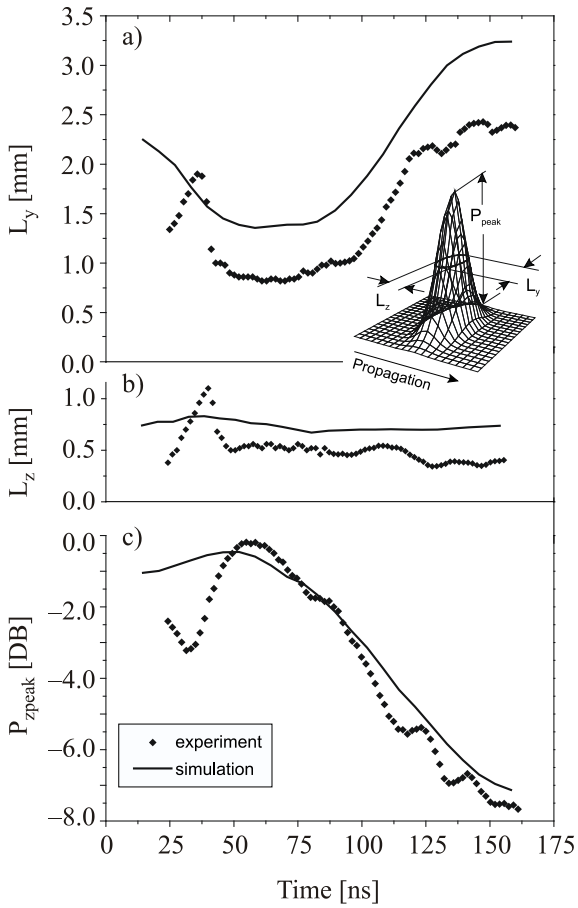

Fig. 2. Widths L_y (a) and L_z (b) at half-maximum power, and normalized peak power (c) of the propagating SW packet shown as functions of the propagation (delay) time t for $T = 29$ ns and $P_{in} = 460$ mW. Symbols: experiment; lines: numerical simulation. From [77].

It is well-known [87], that in the absence of dissipation, two-dimensional self-focusing of an initial wave packet leads to the packet collapse only if the packet's amplitude is sufficiently large for nonlinearity to overcome the effects of diffraction and dispersion. Such a two-dimensional collapse is a threshold process, and it has an amplitude threshold even in a conservative medium. In the presence of dissipation, the amplitude of a self-focusing wave packet decreases exponentially with time, and with the decrease of the amplitude, the focusing effect of nonlinearity also decreases. This leads to a collapse stabilization, and a subsequent defocusing of the packet when its amplitude becomes smaller than the collapse threshold [87].

The influence of dissipation on SW bullets in YIG films is much stronger than the similar dissipative effect on light pulses in optical fibers. Thus, the two-dimensional collapse of dipolar spin waves in YIG films is rapidly stabilized by dissipation, and a quasi-stable SW bullet is formed. Such a bullet propagates for a certain distance without changing its spatial sizes (but constantly losing energy due to dissipation). Then, at some point it starts to diverge in space, when its amplitude is not anymore sufficient for self-focusing. We stress, that an SW bullet is not a stable two-dimensional envelope soliton [51], but a quasi-stable self-focusing wave packet, the collapse of which has been stopped by dissipation.

The evolution of a spectrally narrow two-dimensional (y and z) SW bullet propagating along the z direction in YIG film can be described in the framework of a $(2+1)$-dimensional NLS equation with dissipation (2) (see also [9,27,28,73] and references therein).

In experiment [77] a large (1.8×2.6 cm) sample of a high-quality epitaxial YIG film (thickness $d = 7$ μm, FMR half-linewidth (at 8 GHz) $\Delta H = 0.3$ Oe, saturation magnetization $4\pi M_S = 1750$ G) magnetized to saturation by a tangential bias magnetic field of $H = 2098$ Oe was investigated. A standard delay-line structure with two short-circuited microstrip antennas (length 2.5 mm, width 50 μm) oriented along the y axis, and separated by the distance 8 mm along the z axis, was used for excitation and detection of backward volume magnetostatic spin-wave (BVMSW) packets, as for these waves the magnetic film is a focusing medium along both in-plane directions ($SN < 0$ and $DN > 0$). The carrier frequency of the input BVMSW packet was chosen at $f_c = 7.97$ GHz, 30 MHz lower than the upper boundary of the BVMSW spectrum, to allow propagation of the input pulses of duration $T > 28$ ns without significant distortions to their frequency spectra. The carrier wave number of the BVMSW packet at this frequency point was estimated to be $k_{0z} = 50\ \text{cm}^{-1}$.

In experiment [77] a rectangular microwave input pulse of duration $T = 29$ ns and input power $P_{\text{in}} = 10$–700 mW was applied at the input antenna, which excited a two-dimensional SW packet with an almost cosinusoidal wave amplitude distribution along the y axis, and a maximum amplitude near the center of the antenna. The initial sizes (at half-maximum power) of the input wave packet along the y and z directions were determined by the temporal duration T of the input microwave pulse $v_g T \cong 1.2$ mm, and by the length of the input antenna. The distributions of SW intensity were measured by a space- and time-resolved BLS technique, used in the forward scattering geometry. The spin waves were created in the YIG film by the propagating wave packets, and are proportional to the squared amplitude of instantaneous microwave magnetization. The two-dimensional distributions of propagating SW bullet intensity, corresponding to each delay time, were reconstructed from these time-resolved BLS data collected at each spatial point of the sample.

The experimentally measured two-dimensional distributions of BVMSW intensity for a propagating wave packet obtained with $P_{\text{in}} = 460$ mW, and corresponding to five different delay times, are shown in Fig. 1. The cross sections of the wave packets at the level of half-maximum are shown in the lower part of Fig. 1. The data clearly demonstrates the existence of spatiotemporal self-focusing of the propagating wave packet with the focal point situated near $z = 2 - 2.5$ mm ($t = 50 - 60$ ns), where the peak amplitude of the wave packet has a maximum, and the packet width along the y axis is at a minimum. This effect is further illustrated in Figs. 2(a) and 2(b), where the experimentally measured in-plane sizes L_z and L_y of the BVMSW packet cross sections (at half-maximum power) are shown as a function of the propagation time t for the same input power $P_{\text{in}} = 460$ mW.

For $t < 40$ ns, the BVMSW packet, generated by the microwave field of the antenna, is entering the region of the film accessible by BLS. Therefore, the visible size of the wave packet is linearly increasing with time. For $t = 40$–45 ns, a rapid collapselike self-focusing of the packet is observed along both in-plane directions. Subsequently the collapse is stabilized by dissipation, and in the time interval $50 < t < 100$ ns both in-plane sizes of the propagating packet are almost constant; i.e., a quasi-stable SW bullet is propagating in the film. For $t > 100$ ns, the transverse size L_y of the packet starts to increase rapidly due to the influence of diffraction. The dependence of the normalized peak power $P_{\text{peak}} / P_{\text{peak}}^{\max}$ of the wave packet on the propagation time for the input power $P_{\text{in}} = 460$ mW is shown in Fig. 2(c). The above-described spatiotemporal self-focusing effect was observed for $P_{\text{in}} > 100$ mW. For lower input powers, a monotonous decay of the packet peak amplitude, and also a monotonous increase of both packet sizes L_y and L_z with the increase of propagation time are observed.

The next step in the investigation of the nonlinear SW packets was a study of their collision properties [88,89]. In these papers it was demonstrated both experimentally and by numerical simulations that SW solitons retain their shapes after collisions with other SW solitons only in a one-dimensional case. In contrast, in the two-dimensional

case the SW bullets loose this solitonic properties and suffer an almost complete destruction in a collision with a similar SW bullets.

In [88] SW bullets were experimentally observed and visualized in a system of BVMSW propagating along the direction of the bias magnetic field in a tangentially magnetized YIG film. The experiment shows that in a wide YIG film sample, where the transverse size of the medium is essentially unrestricted, a strong two-dimensional self-focusing of propagating SW packets takes place. With the increase of the propagation time, the initially elliptical cross sections of the propagating SW bullet becomes much narrower, and almost circular (Fig. 3(b)), which is a well-known feature of wave packets approaching collapse. The collapse, however, is stopped by dissipation, and a quasi-stable two-dimensional SW bullet is formed (Fig. 3(b)). At the collision point the increase of the combined intensity in the two colliding SW packets leads to a catastrophic self-focusing and collapse (Fig. 3(c)) that cannot be stabilized by dissipation. Thus, the equilibrium between the self-focusing and dissipation, responsible for the quasi-stability of two-dimensional SW bullets shown in Fig. 3(b), is broken, and both SW bullets are destroyed in the collision process. The intensity of the two initial SW packets is spread across the whole measurement area (see Fig. 3(d)).

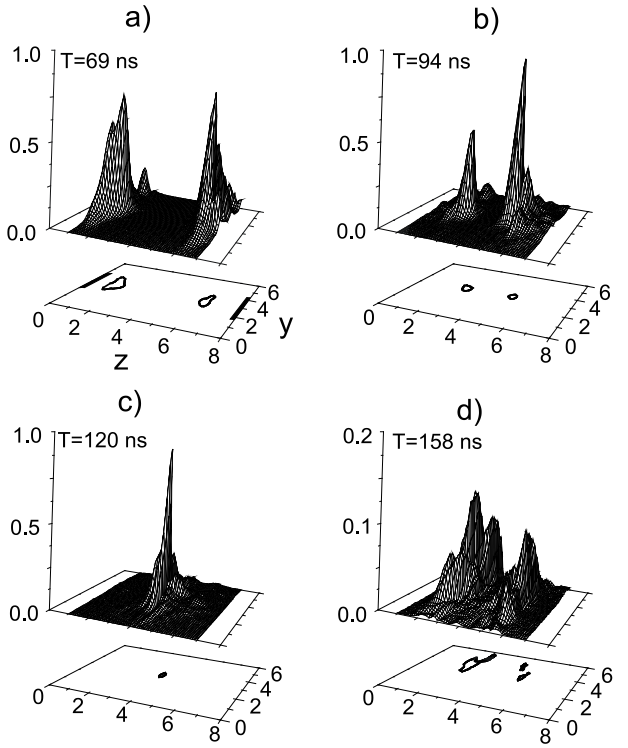

Fig. 3. Formation and collision of two-dimensional self-focused SW bullets in a wide YIG film sample. The upper frames ((a), (b)) show the two-dimensional intensity distribution of the propagating wave packets, corresponding to four different values of the propagation time as indicated. The lower frames ((c), (d)) show the packet's cross sections at the half-maximum level. The black stripes in (a) show the positions of the microstrip antennas. From [88].

The qualitative difference between the collision properties of quasi-one-dimensional SW envelope solitons in the YIG waveguide, and two-dimensional SW bullets in a wide YIG film is further illustrated in Fig. 4 where the transverse (L_y) and longitudinal (L_z) widths of propagating SW packets are presented as functions of t, the propagation time. The first 100 ns is a period of soliton formation (Figs. 4(a) and 4(b)), during which the shape of the propagating SW packet becomes elliptical and elongated along the y direction ($L_y / L_z \approx 2.5$). It is clear that after the initial period of soliton formation, the spatial sizes of the resulting SW soliton remain nearly constant and are not significantly affected by the collision with the other soliton, which takes place at $t = 165$ ns. The behavior of the two-dimensional SW bullet in a wide film (Figs. 4(c) and 4(d)) is quite different. By the end of the initial period $t < 80$ ns, during which a strong two-dimensional self-focusing leading to SW bullet formation takes place, the propagating two-dimensional SW bullet becomes very narrow and almost circular ($L_y / L_z \approx 1$). A subsequent collision with the other bullet at $t = 120$ ns leads to a dramatic increase of the bullet's sizes along both in-plane directions, and to the bullet's destruction at $t = 140$ ns (see Figs. 4(c) and 4(d)).

Thus, the above presented experimental data and numerical study results clearly demonstrate that while a two-dimensional SW bullets in a wide YIG film sample appear to be stable and preserve their size and shape in a certain range of propagation distances, in reality they are only quasi-stable, as they suffer almost complete destruction in a collision with another SW bullets.

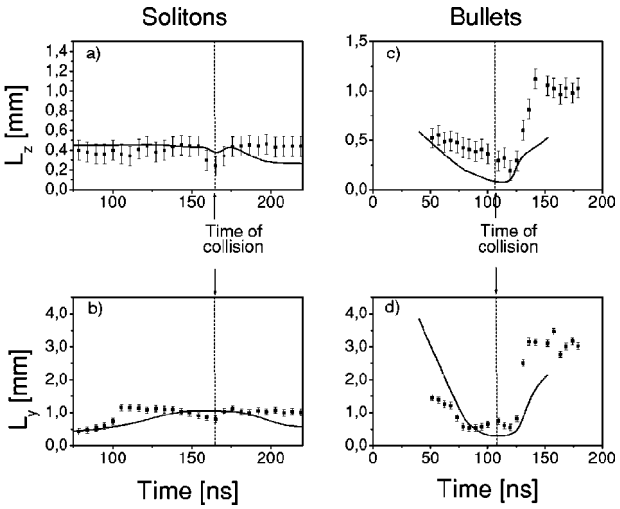

Fig. 4. Widths L_z and L_y of the SW packets propagating from left to right, measured at half-maximum level, as functions of the propagation time: (a) and (b) in YIG waveguide; (c) and (d) in a wide YIG film. Note, that the collision moments shown by vertical broken lines are different in a waveguide (165 ns), and in a wide film (120 ns). Experimental results are shown by symbols with error bars, while numerical results are shown by solid lines. From [89].

The experimental observation of self-generation of SW bullets in an active ring was performed in [90]. The ring was composed of an YIG film with two antennas for wave packets excitation and detection, and a microwave amplifier connecting the antennas and closing the ring. The system forms a transmission line for two-dimensional BVMSW wave packets, and no external coherent input signal was applied to the antennas. The transmission line itself plays the role of a resonator in a feedback loop of a standard microwave generator. The resonance frequencies of a ring are determined by standard phase matching conditions.

To achieve stable generation of a SW pulse sequence, it is necessary to fulfill several conditions. First, the frequency passband of the ring (which includes the amplifier and the YIG film transmission line) must be larger than the width of the central lobe of the frequency spectrum of a single generated pulse. Otherwise, the shape of the pulse will be distorted due to the filtering properties of the ring. It is known [77] that the duration of a SW bullet formed from a coherent nonlinear input pulse of about $\tau = 15$–20 ns. Thus, a transmission line with a passband of $\Delta F = 150$ MHz is used, providing $\tau \Delta F \geq 2$.

Second, the amplification gain of the external amplifier must be large enough to compensate for the losses in the ring and to allow for self-generation. Finally, for the generation of substantial nonlinear pulses in the ring, it is necessary to choose a distance between the antennas larger than the characteristic nonlinear length in the medium [90]. This will allow for the development of both longitudinal and transverse focusing. The nonlinearity also provides a phase-locking mechanism for the generated harmonics.

Space- and time-resolved BLS technique in the forward geometry is used to monitor the propagation of the nonlinear wave packets. This allows us to obtain two-dimensional distribution of the SW intensity (proportional to the squared amplitude of the local dynamic magnetization in the film) of the propagating wave packet with a spatial resolution of 0.1 mm and a temporal resolution of 2 ns.

A peak power of generated wave packet is achieved when the input antenna is driven at $P_1 = 220$ mW. At this power, there is clear self-focusing in both in-plane directions of the generated wave packet, and a formation of a SW bullet. The experimentally measured parameters of this bullet (width, length, peak power) are very close to the parameters of a BVMSW bullet formed under coherent excitation by an external input microwave pulse [77].

The time evolution of the self-generated SW packets shows that for the case of the weak nonlinear regime, $P_1 = 1$ mW, after a small initial self-focusing of the packet taking place for $t < 45$ ns, the packet is only weakly spread by diffraction in its further propagation. In contrast, in the strongly nonlinear regime, just before the onset of the chaotic behavior, when $P_1 = 220$ mW, a significant transverse self-focusing is observed for $t < 52$ ns. For $55 < t < 70$ ns the wave packet propagates as a well-formed bullet exhibiting an almost constant transverse width of about 0.65 mm. This is the region where the self-focusing two-dimensional SW packet becomes quasi-stationary due to the loss of energy to linear dissipation. With the further increase of the propagation distance dissipation continues to reduce the bullet's amplitude (thus reducing the focusing action of nonlinearity), and, in the end, diffraction uncompensated by nonlinearity spreads the wave packet in the transverse direction and causes the increase in width L_y. The dispersion acting in the direction of propagation has a similar (but weaker) effect on the packet's length L_z. This behavior of the self-generated SW bullet is very similar to the behavior of coherently excited SW bullet [77].

Thus, the observed self-generation process provides unambiguous evidence that SW bullets are intrinsic excitations of a two-dimensional nonlinear magnetic medium with dissipation that is focusing in both directions.

After detailed studies of generation, propagation and interaction of SW bullets, a parametric interaction of two-dimensional SW packets with quasi-uniform pulsed pumping was performed in [91] using the same BLS experimental technique as in [90] combined with a spatially localized SW parametric amplifier embedded in the YIG-film waveguide [64,92–94]. Two-dimensional maps of the SW intensities (proportional to the local values of the squared dynamic magnetization in the film) were recorded with spatial resolution of 0.1 mm and temporal resolution of 2 ns (Fig. 5). The upper panel of Fig. 5 demonstrates the evolution of a two-dimensional wave packet of duration $\tau = 30$ ns after it has been launched from the antenna and before it reaches the pumping area. The initial width of the packet (determined by the antenna length and the carrier wave number) was $L_y = 0.4$ mm, the power of the initial microwave pulse defining the intensity of the packet was $P_{in} = 146$ mW. As it can be seen in Fig. 5 the packet spreads along the transverse (y) direction during propagation due to the strong diffraction in the film.

The lower panel of Fig. 5 demonstrates the propagation and evolution of the reversed ($\mathbf{k}' = -\mathbf{k}$) wave packet formed as a result of the parametric interaction [64,92]. It is

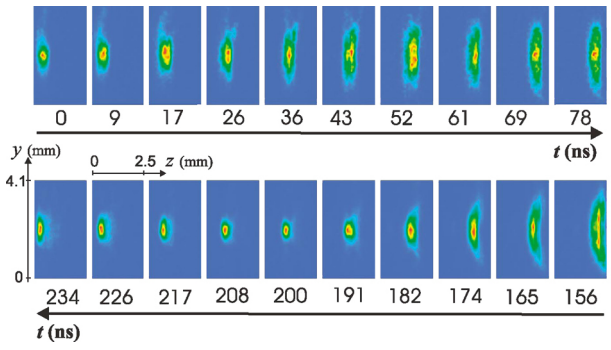

Fig. 5. (Color online) The spatial distributions of the SW pulse intensity captured at successive moments of time both for incident (upper part) and for reversed (lower part) SW packets. $P_{in} = 146$ mW. From [91].

clear that the strongly amplified reversed wave packet experiences a pronounced nonlinear two-dimensional self-focusing, which leads to the formation of a SW bullet (see frames corresponding to 191, 200, and 208 ns). The same effect was observed for the strongly amplified initial SW packet, which passed through the pumping area in the forward direction.

One can see from Fig. 5 that the reversed packet undergoes a wave-front reversal (phase conjugation). The wave front of the incident pulse that is slightly concave immediately before the interaction with pumping (frame corresponding to 78 ns) becomes clearly convex after the interaction (156 ns) (note the change of direction of propagation between these two frames). This effect of two-dimensional wave-front reversal, which was realised in this experiment for the first time, was even more pronounced for a linear, low-power input wave packet, where it was not superimposed by the bullet formation process.

Thus, paper [91] revealed that the SW bullets, being two-dimensional intrinsic excitations of a nonlinear diffractive and dispersive medium with dissipation, can be generated parametrically in magnetic films from linear input wave packets. They are formed from both the forward-propagating and reversed wave packets, and their properties are similar to the properties of SW bullets generated by other means.

In contrast to the SW bullet in continuous YIG film, the SW bullet in a narrow YIG film stripe (playing the role of a bullet waveguide) was investigated in [95]. The formation of a quasi-2D nonlinear guided SW bullet in longitudinally magnetized stripes of YIG film was experimentally observed by using time- and space-resolved BLS spectroscopy and confirmed by numerical simulation. It was revealed that such SW bullet represent stable SW packets propagating along a waveguide structure, for which both transversal instability and interaction with the side edges of the waveguide are important. The experiments and the numerical simulation of the evolution of the SW excitations have shown that the shape of the formed packets and their behavior are strongly influenced by confinement conditions. Namely, a specific magnetostatic effect — the effective dipole pinning of the magnetization at the edges of the stripe, the width-mode group velocity matching of different discrete waveguide modes, and the extension of the width-mode spectrum due to nonlinear mode-mode energy transfer are essential for the nonlinear evolution of the initial SW excitation. Both the experimentally detected properties of the evolution and the theoretically revealed mechanism of formation show that the observed "guided spin-wave bullets" are specific for laterally confined magnetic films.

A detailed study of a collapsing SW bullets in a YIG film was done in [96]. It was shown that a (2+1)-dimensional wave packet, like SW bullet, in a medium with cubic nonlinearity and a two-dimensional dispersion is intrinsically unstable, and undergoes nonlinear narrowing leading to collapse as nonlinearity overcompensates linear broadening due to 2D parabolic dispersion. Weak magnetic losses in a real magnetic film may balance the nonlinear narrowing. This results in a quasi-2D spatially localized bell-shaped waveform called a bullet and ensures its stability for some distance of propagation. The stable bullets are observed in a certain range of initial powers for the wave packets. For larger input powers, waveform collapse is unavoidable.

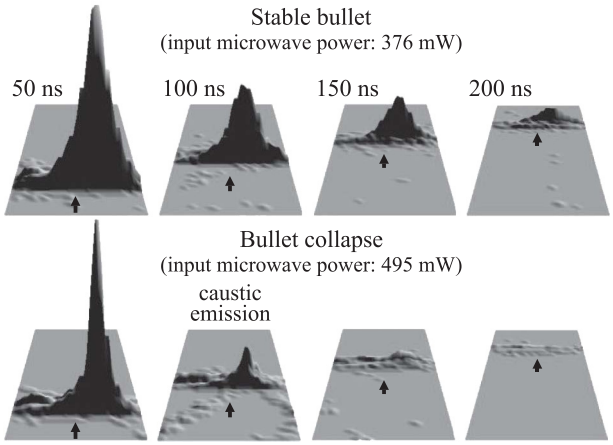

Fig. 6. Snapshots of SW packets measured at different input powers and at 50 ns time intervals. Arrows show the bullet propagation direction. It coincides with the direction of the bias magnetic field **H** and the coordinate axis *z*. From [96].

In the experiment [96], when the power increases beyond the range of bullet stability, the wave packet collapses, and the most prominent feature of a wave collapse are seen. A pair of rays irradiated from the packet in the backward direction (second panel in the lower row of Fig. 6). It was revealed that the rays have narrow apertures and are directed at well defined angles to the longitudinal axis of the ferromagnetic stripe (the value of the angle between the rays is 64°). The performed numerical simulation proves that the observed effect is the fundamental phenomenon of wave emission from collapsing packets in materials with cubic nonlinearity and 2D dispersion of an order higher than parabolic. In addition, since the ferromagnetic-film medium used in the present study is also characterized by a uniaxial anisotropy, the observed radiation takes the form of narrow-aperture beams of continuous waves at very specific angles to the bullet propagation direction. This specific effect of radiation of untrapped waves along the caustic directions may exist for other 2D media as well, provided uniaxial anisotropy of dispersion is available or induced in the medium [97–101].

3.2. Spin-wave bullets in nanoscale oscillators

At almost the same time when SW bullets were observed in magnetic films [77] another important discovery was made. It has been theoretically predicted [47,48] and

experimentally observed [102–109] that spin-polarized current passing through a thin "free" magnetic layer (FL) of a magnetic bi-layered structure, can excite microwave magnetization oscillations. So, a concept of a spin-torque nano-oscillator (STNO) has been developed.

A theory explaining many experimentally observed features of this phenomenon was developed in a series of theoretical papers [110–113], but the physical nature of a dynamic SW mode excited in an in-plane magnetized magnetic current-driven nanocontact was determined in [29].

In [29] a spatially nonuniform nonlinear theory of SW excitations driven by a spin-polarized current in an in-plane magnetized magnetic nanocontact (NC) was developed, and it was found that such an excitation is an SW bullet. It was assumed that the free ferromagnetic layer of a nanocontact is infinite in the $y-z$ plane, and has a finite thickness d in the x direction (d is assumed to be sufficiently small to consider that the magnetization **M** is constant along the FL thickness, and that the dipole-dipole interaction can be described by a simple demagnetization field). It was also assumed, that the internal magnetic field consisted of the bias and the interlayer exchange fields applied in the z direction in the film plane. Using a standard Hamiltonian SW formalism [8], an approximate Eq. (3) for the SW excitation amplitude was obtained. In the considered case of an in-plane magnetized FL the nonlinear coefficient N is negative, and the nonlinearity and dispersion satisfy the Lighthill criterion $ND<0$. Thus, Eq. (3) had a nonlinear self-localized radially symmetric solitonic solution in the form of a standing SW bullet: $c(r,t)=$ $=C_0\psi(r/\ell)\exp[-i\omega t]$, where the dimensionless function $\psi(x)$ describes the profile of the SW bullet, and has to be a localized solution of the equation $\psi''+x^{-1}\psi'+\psi^3-\psi=0$. C_0, ℓ, and ω are the characteristic amplitude, characteristic size, and frequency of the bullet, respectively.

Among these three parameters only one is independent. Taking the amplitude C_0 as an independent parameter, one can express the two other parameters as $\omega=\omega_0+NC_0^2$, $\ell=\sqrt{|D/N|}/C_0$.

It should be stressed, that the frequency of the SW bullet lies below the linear frequency ω_0 of the FMR, i.e., outside the spectrum of the linear spin waves.

This is the main reason for the self-localization of the SW bullet, as the effective wave number of the SW mode with the frequency ω lying below the FMR frequency is purely imaginary.

The developed theory shows that the frequency of the SW bullet is shifted by the nonlinearity below the spectrum of the linear spin waves, and, therefore, this nonlinear mode has an evanescent character with the vanishing radiative losses, which leads to a substantial decrease of the threshold current I_{th} of its excitation in comparison to the threshold current necessary to excite a linear propagating SW mode [110].

In the main panel of Fig. 7 the comparison of the predictions of the developed bullet model [29] with the results of the experiment [108] for the magnitude of the SW frequency generated at the threshold as a function of the applied magnetic field was demonstrated. It is clear, that the bullet model gave a quantitative description of the experiment. In the inset of Fig. 7, the theoretical dependence of the generated frequency on the bias current calculated from the bullet model in the above-threshold regime, was compared with the experimental data taken from [108]. It can be seen, that the theoretical curve was nonlinear, and agreed with the experiment, demonstrating a qualitative linear decrease of frequency with current. This was attributed to the fact, that the developed model was correct only at a threshold and slightly above it, and a more sophisticated nonlinear model containing higher-order nonlinearities is needed to achieve a full quantitative agreement with experiment in the strongly nonlinear above-threshold regime.

Detailed micromagnetic simulations [114] have proven that a current-driven in-plane magnetized magnetic NC can support at least two different types of microwave SW modes: a quasi-linear propagating "Slonczewski" mode [47] and a subcritically-unstable self-localized nonlinear SW bullet mode [29]. In [115] it was shown that in a spin-torque microwave oscillator based on a magnetic NC, the nature of the microwave SW mode generated at the threshold critically depends on the angle between the external bias magnetic field and the plane of the FL. When the external

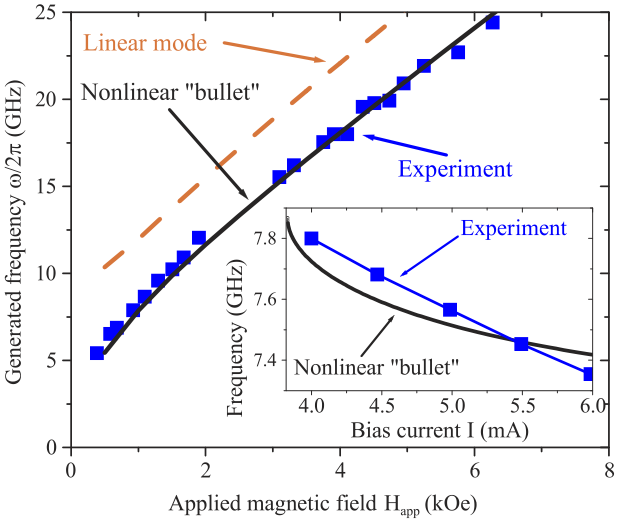

Fig. 7. (Color online) Dependence of the frequency ω, generated at the threshold, on the applied magnetic field H_{app}. Solid line — frequency of the nonlinear bullet, dashed line — frequency of the linear mode, symbols — experiment. The inset shows the dependence of the generated frequency on the bias current for H_{app} = 1 kOe: solid line — nonlinear bullet, symbols — experiment. The parameters are: $4\pi M_0$ = 8.0 kG, H_{app} = 1 kOe, $H_{ex}=0$, $A=1.4\cdot10^{-6}$ erg/cm, α_G = 0.02, d = 5.0 nm, R_c = = 20 nm, ε = 0.25, spectroscopic Lande factor g = 2. From [29].

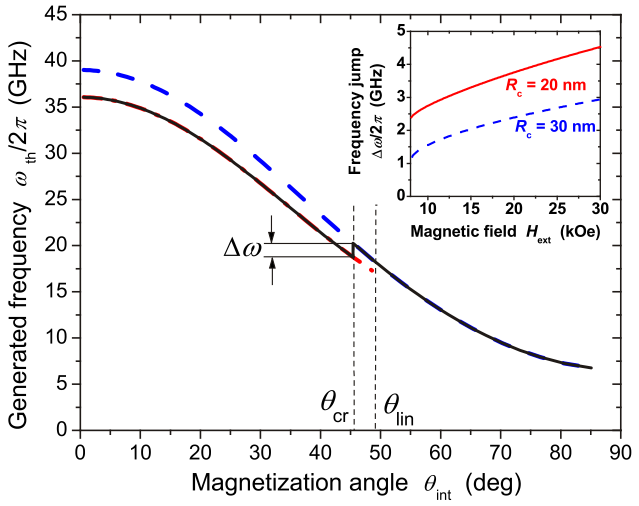

Fig. 8. (Color online) Main panel: Dependence of the frequency generated at the excitation threshold on the out-of-plane angle of the internal bias magnetic field θ_{int}. The dashed line shows the frequency of the linear mode, the dash-dotted line the frequency of the nonlinear bullet. Vertical dashed lines show magnetization angles θ_{cr} and θ_{in}. The parameters are $4\pi M_0 = 8$ kG, $H_{ext} = 10$ kOe , $\lambda_{ex} = 5$ nm, $L = 5$ nm, $\alpha_G = 0.02$, $\varepsilon = 0.3$. Inset: Dependence of the frequency jump $\Delta\omega$ at $\theta_{in} = \theta_{cr}$ (see main panel) on the magnitude of the external bias magnetic field H_{ext} for two different nanocontact radii: $R_c = 20$ nm (solid line) and $R_c = 30$ nm (dashed line). From [115].

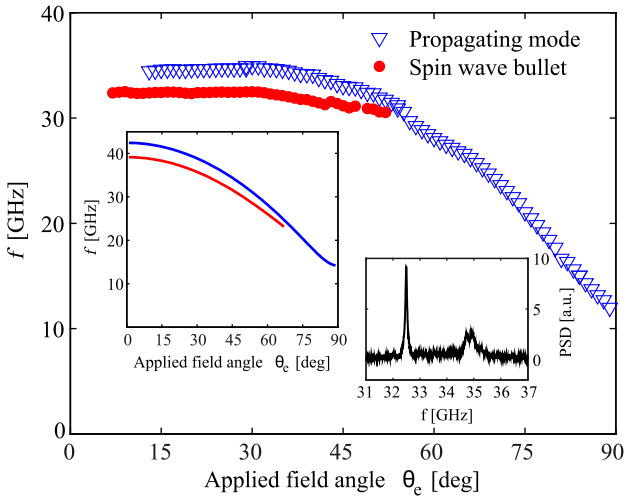

Fig. 9. (Color online) Measured frequencies of the observed SW modes as a function of the applied field angle θ_e at $I = 14$ mA and $\mu_0 H_e = 1.1$ T. Left inset: theoretically calculated frequencies of the propagating (upper curve) and bullet (lower curve) modes at the current threshold, for nominal parameters of the nanocontact STNO. Right inset: power spectrum at $\theta_e = 30^\circ$, $I = 14$ mA. From [33].

bias field rotates from normal to in-plane orientation, an abrupt transition from a propagating cylindrical wave with a frequency higher than the frequency of the linear FMR to a self-localized standing nonlinear SW bullet with the frequency lower than the FMR frequency takes place at a certain intermediate angle. This transition manifests itself as an abrupt jump (of the order of several gigahertz) in the generated microwave frequency (Fig. 8). This mechanism of the mode switching might explain abrupt jumps of the generated microwave frequency observed in recent experiments on spin-torque oscillators. Additionally, in [116] it was shown that the maximum angle of the external bias magnetic field from the film plane at which the nonlinear bullet mode can exist is $\theta_{in} = 77^\circ$ in the analytical approach, and $\theta_{in} = 62^\circ$ in the micromagnetic simulations.

Experimentally the angular dependence of the SW excitations in NC-based spin-torque oscillators was studied in [33,36]. There were, however, some notable differences between the theory [29] and experiments [33]. The most striking feature was the simultaneous excitation of both linear and SW bullet modes (Fig. 9). Such a co-excitation was not supported neither by the theory [29,115], nor by the micromagnetic simulations [114,116]. In contrast, a hysteresis between the two modes was predicted by the theory. The effect of the mode coexistence can be explained by taking into account the large Oersted field generated by the bias current flowing through the NC, which was ignored in the analytical theory [29,114–116], but was accounted for in the micromagnetic simulations in [33,117] which demonstrated a good agreement with the experimental results [33,36].

An additional experimental evidence showing the existence of SW bullets was provided by V.E. Demidov and co-authors using the BLS technique, which allowed them to perform a direct observation and mapping of spin waves emitted by a STNO [34]. These results were also extended in the recent paper [118].

The investigations of SW bullets in spin-Hall nano-oscillators (SHNOs) were carried out in recent papers [119–121]. In [119] it was found, that a synchronization of an SW bullets to an external driving microwave signal exhibits a threshold determined by the magnetic fluctuations pumped above their thermal level by the spin current. This process was significantly influenced by the nonlinear self-localized nature of the auto-oscillatory mode.

To characterize the synchronization process in [119], the dependence of the synchronization frequency interval Δf_S was measured as a function of the dynamic microwave magnetic field h, which is proportional to the square root of the driving microwave power P. The dependence of Δf_S on $P^{1/2}$ obtained at different values of dc current are shown by symbols in Fig. 10(a).

No synchronization was observed at microwave powers below $P_{th}^S = 0.03$ mW, regardless of the dc current value. At a current $I = 18$ mA (which is significantly above the oscillation onset), Δf_S exhibits an approximately linear dependence on $P^{1/2}$ above the threshold P_{th}^S (circles and solid straight line in Fig. 10(a)), while at the smaller currents (close to the oscillation onset), a rapid increase of

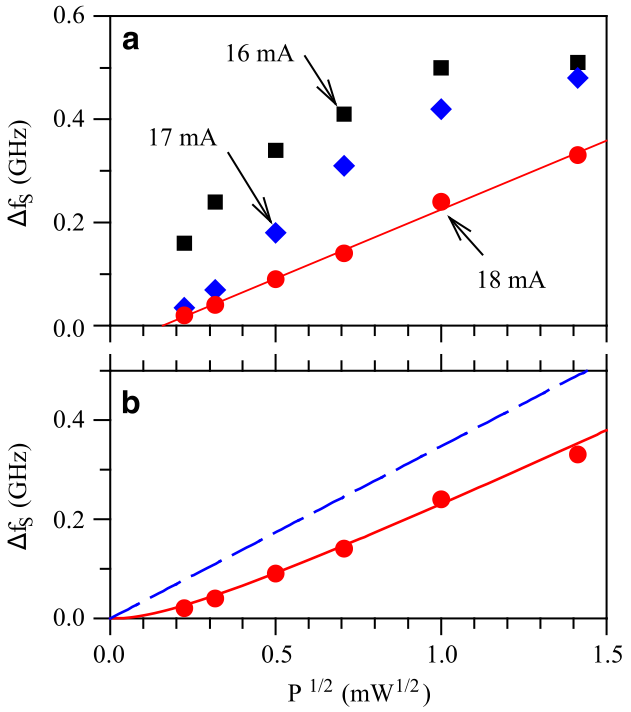

Fig. 10. (Color online) Dependence of the synchronization interval on the dynamic field. (a) Measured synchronization interval versus $P^{1/2}$, at the labeled values of dc current I. Solid line is a linear fit of the I = 18 mA data. (b) Symbols: measured synchronization interval versus $P^{1/2}$, at I = 18 mA. Solid curve: calculated synchronization interval in the presence of noise. Dashed curve is the same dependence calculated in the absence of noise. The experimental data were obtained by BLS. From [119].

Δf_S at small microwave power is followed by a saturation (squares and diamonds in Fig. 10(a)).

The observed behavior of the synchronization frequency interval Δf_S is not described by the theory of synchronization of nonlinear single-mode oscillators [26], which predicts a universally linear dependence of Δf_S on $P^{1/2}$. Also [119] shows that the observed synchronization threshold could be explained by the effects of the thermal noise enhanced by the spin current on the self-localized SW bullet. This analysis was based on the theory of auto-oscillator synchronization developed in [26], applying it to the bullet oscillation mode of the SHNOs [29], and analytically taking into account the effect of thermal noise that was introduced numerically by Georges *et al.* [122].

It was noted in [119] that the synchronization (or injection-locking) of a well-developed SW bullet observed at dc currents close to I_C (see I = 16 and 17 mA data in Fig. 10(a)) cannot be quantitatively described by the theoretical dependence of Δf_S on $P^{1/2}$.

The authors in [119] identify two mechanisms responsible for this disagreement. First, the assumption of the SW mode rigidity used in the analysis of [119] does not hold for small oscillation amplitudes, since the external perturbations can make a significant contribution to the energy balance of the bullet mode. Second, the approximation of the uncorrelated white noise is not valid in this regime, as the non-equilibrium populations of the magnetic modes deviate significantly from the thermal distribution in the vicinity of the damping compensation point. On the other hand, at larger currents one can expect that the stronger nonlinear effects result in more efficient thermalization of spin waves.

Another experimental observation of the mutual synchronization of the SW bullet-based magnetic nano-oscillators driven by a pure spin current generated by nonlocal spin injection was reported in [121]. It was shown there, that the oscillators efficiently synchronize due to the direct spatial overlap of the dynamical modes excited by the spin current, which was facilitated by the large size of the auto-oscillation area inherent to these devices. The synchronization occurred within an interval of the driving current values determined by the competition between the dynamic nonlinearity. The demonstrated synchronization effects can be utilized to control the spatial and spectral characteristics of the dynamical states induced by the spin currents.

A strong SW localization in the center of the YIG sample was recently observed in [120], indicating the formation of a nonlinear, self-localized SW bullet. It was demonstrated, that the concept of a spin-torque-FMR can be extended to the magnetic insulators, where the formation of a nonlinear, self-localized SW modes driven by an alternating current can be observed. The authors of [120] used an electrically-driven spin-torque-FMR excitation and detection scheme in a bi-layered structure YIG / heavy normal metal (Pt), that was originally developed for the all-metallic systems.

4. Droplets in magnetic films and nanostructures

After A.M. Kosevich's pioneering works [17,22], where the first prediction of conservative droplet solitons was made, droplets in magnets were not experimentally observed until 2013 [79]. This first droplet observation has been carried out using NC–STNOs based on orthogonal pseudo-spin-valve stacks, where the magnetization of the Co fixed layer lies in-plane at a zero applied field, and the magnetization of the FL (made of a Co/Ni multilayer) is along the film normal, because the perpendicular magnetic anisotropy (PMA) in the FL is sufficiently strong to overcome the demagnetization field.

The field dependence of the microwave signal from a NC–STNO with 63-nm NC diameter in low to moderate perpendicular fields (Fig. 11(A)) have shown, as expected, a linear FMR-like field dependence [79]. However, at a critical field of $\mu_0 H_{\text{droplet}} = 0.65$ T (μ_0 is the vacuum permeability), the precession frequency exhibited a dramatic drop to a frequency between the Zeeman and FMR frequencies, with a simultaneous jump in the integrated power (P). A similarly dramatic transition can be observed (Fig. 11(B)) as a function of current in a constant 0.8 T field with similar changes in frequency and power. The field-dependence

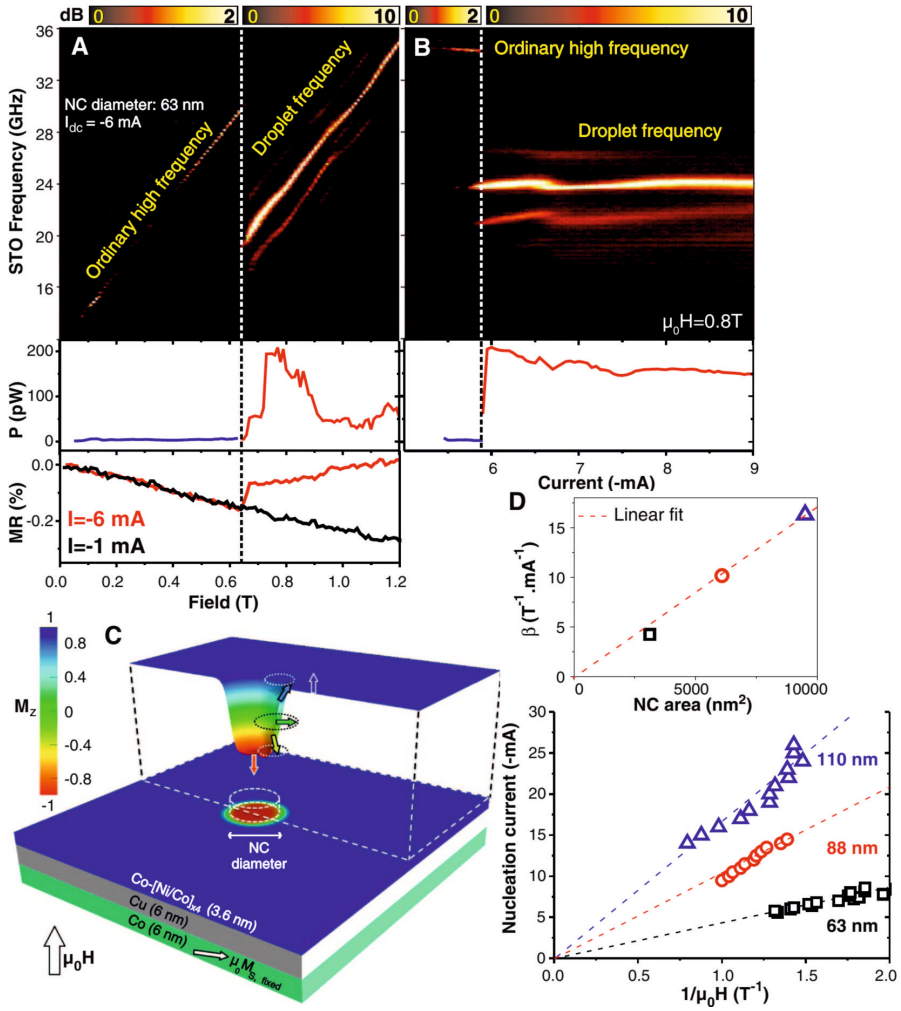

Fig. 11. (Color online) (A) Frequency, power P, and magnetoresistance MR as a function of perpendicular field at $I_{dc} = -6$ A (and also −1 mA for the MR data) for a 63 nm NC–STO. Below 0.65 T, the FMR-like signal increases linearly as 28.7 GHz/T, whereas MR decreases with —0.25%/T. At $\mu_0 H_{\text{droplet}} = 0.65$ T, the frequency drops by 10.3 GHz, modulation sidebands appear, and P jumps from 5 to 200 pW in two steps. MR experiences a jump at the same field followed by an increasing trend of +0.17%/T. (B) Current sweep of the same device at $\mu_0 H = 0.8$ T. At $I_{\text{droplet}} = -5.8$ mA, the frequency again drops by 10 GHz, modulation sidebands appear, and P jumps from 5 to 200 pW. The modulation frequency shows a stronger current dependence, and a faint second-order lower band becomes visible at ∼−8 mA. (C) NC–STO on Co/Cu/Co-[Ni/Co]$_{\times 4}$ orthogonal spin-valve with a cross section of a reversed magnetic droplet shown on top. Arrows surrounded by dotted circles indicate precession mechanism of droplet perimeter. (D) I_{droplet} determined from MR measurements for three different NC diameters d_{NC}: 63, 88, and 110 nm. Dashed lines indicate fit for $I_{\text{droplet}} = \beta(d_{NC}) \cdot (1/H)$. Inset: $\beta(d_{NC})$ versus NC area together with a linear fit. From [79].

of the magnetoresistance $\text{MR} = [R(H) - R(H=0)]/R(H=0)$ (R is the device resistance) was also measured both at −6 mA and at a lower current of −1 mA (inset in Fig. 11(A)).

With the aid of the dissipative droplet theory [80,81] and micromagnetic simulations, the authors of [79] studied a complex magnetization dynamics with different dynamical wave states, including quasi-periodic and periodic oscillations (Fig. 12). A dramatic drop in frequency at the droplet nucleation, was identified as a point of droplet formation [80], when all the spins in the droplet precess uniformly at a single fixed frequency substantially lower than the frequency of the linear excited mode (Fig. 12(a)). In [80], a droplet drift instability was identified, when a droplet was ejected from the area of a nanocontact (NC), eventually succumbing to damping, and leaving room for the nucleation of a new droplet in a periodic fashion. This process occurs on a nanosecond time scale, which is consistent with the experimentally observed modulation sidebands. The drifting droplet may experience a restoring force leading to gyrotropic-like motion of the droplet within the NC area with a characteristic ∼1 GHz frequency (Fig. 12(b)). Depending on the system parameters, micromagnetic simulations also reveal asymmetric droplets that "spin" at the edge of the NC area, while emitting spin waves (Fig. 12(c)).

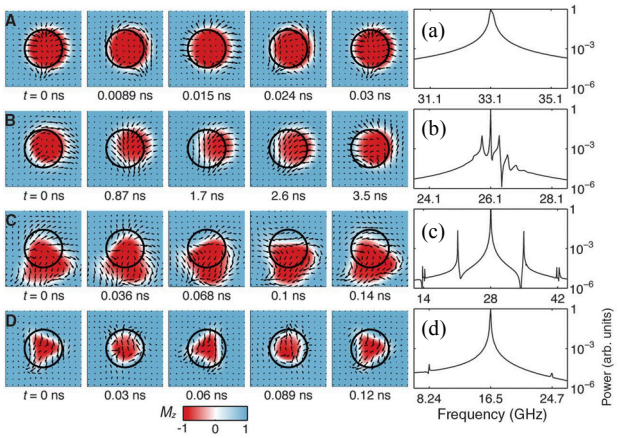

Fig. 12. (Color online) Time sequences of out-of-plane, M_z (in color), and in-plane (vector field) magnetization component of free layer from micromagnetic simulation. (Right) The power spectrum associated with the NC averaged projection of magnetization onto the polarization layer. Parameters are given as triples (field, NC diameter, and current). (a) Stationary droplet precession with a single spectral peak for large field (1.1 T, 80 nm, and –12 mA). (b) Droplet oscillation leading to prominent sidebands for moderate field (0.8 T, 63 nm, and –8 mA). (c) Spinning of an asymmetric droplet for moderate field (0.9 T, 50 nm, and –9 mA). (d) Droplet perimeter deformations (breathing) with period twice the precessional period (0.5 T, 80 nm, and –8 mA). From [79].

For a strong canting of the polarizer away from the film normal (weak bias magnetic fields), the authors of [79] observed periodic dynamics with signals at 1/2 and 3/2 of the fundamental droplet frequency (Fig. 12(d)). These characteristic signals can be identified with a breathing mode whose observed breathing frequency is half the precessional frequency in the droplet. The authors of [79] believed that the observed magnetic droplet may have an impact on applications, in particular, it may have an influence on the emerging fields of STNOs, domain-wall electronics, and magnonics. The authors of [79] mentioned, that for STNOs the dramatic frequency drop enables ultra-broadband frequency-shift keying, in which the carrier frequency can be switched by ~ 10 GHz by varying the drive current a fraction of its absolute value.

In the time period between the droplet prediction [17,22] and the experimental observation [79], there were several theoretical studies of magnetic solitons. The theoretical papers by M.A. Hoefer and co-authors played an important role in these studies. A general theory of conservative and dissipative droplets in NCs was developed in [80], and perturbations and nucleation of the dissipative droplets were also considered. This theory was, then, applied to the analysis of propagation and control of nanoscale magnetic-droplet solitons [81,82]. The modulation of magnetic droplet solitons, attraction, merger, reflection, and annihilation in their scattering were considered in [83] and [84], respectively, while the drift instability and stochastic thermal perturbations of magnetic dissipative droplet solitons were considered in [123]. Also, a mathematically strict perturbation theory for propagating magnetic droplet solitons was presented in [85]. Using this theoretical basis, a simple theory for the conservative droplet soliton was also developed in [124]. In addition, during this time several papers involving micromagnetic simulations of droplets were made [125–127] which agree quite well with experiments [79,126–131].

In [129], it was shown that at low temperature a reversal of the droplet magnetization can occur. However, room-temperature measurements proved, that there is an abrupt threshold in both current and field at which the droplet excitations occurred, and showed that spin-precession frequencies in droplets were substantially below the FMR frequency [79,126]. However, there was no direct experimental evidence for a fully reversed magnetization state beneath the current-driven NC.

In [128] the annihilation of droplet excitations was studied through a dc measurements of resistance. The applied field was fixed perpendicular to the film plane while sweeping the applied current. The measurements showed an abrupt increase in the resistance when a droplet forms with the increase of current, and an abrupt decrease in the resistance when the droplet annihilates with the current decrease. Figure 13(a) shows the resistance curves as a function of the current at different fields. At each field, the cur-

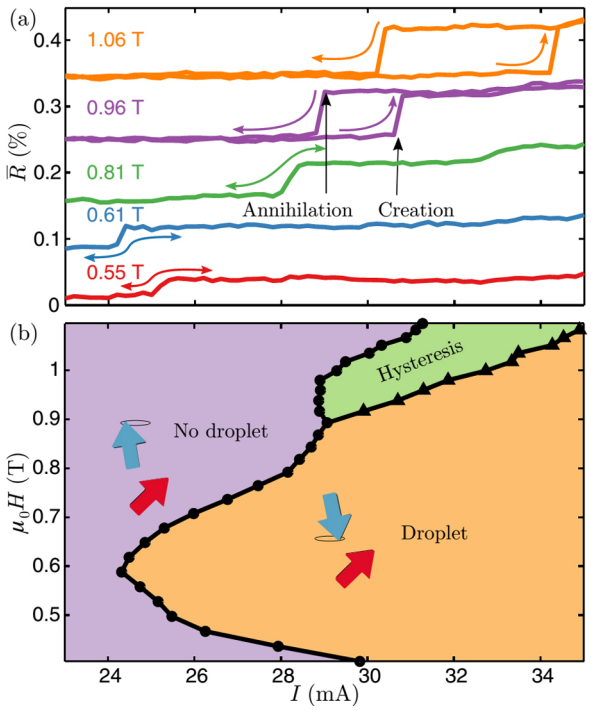

Fig. 13. (Color online) (a) Measured normalized resistance $R = R / R_P$ as a function of applied current for fields ranging 0.5 – 1.1 T. Curves are offset for clarity. (b) Stability map of the droplet soliton: in the hysteretic area, triangles show creation of the droplet, and dots annihilation. From [128].

rent was swept up to 35 mA, and, then, back down to 0. Although the authors detected the onset of the excitations at fields 0.5 T $< \mu_0 H <$ 0.9 T, it was not until larger field values, $\mu_0 H >$ 0.9 T, that a hysteresis phenomena was observed: while sweeping the current up, the droplet creation occurred at higher currents than the annihilation when sweeping it down. Figure 13(b) is a state map plot representing creation and annihilation currents for all measured fields.

In contrast with the hysteresis observed and characterized at low temperature [129], the room-temperature measurements showed much smaller hysteretic effects [79]. The authors of [128] noted, that, although the onset maps for the droplet excitations were almost identical, the hysteretic responses were considerably different: all samples showed hysteresis at larger fields, $\mu_0 H >$ 0.9 T, but the size of the hysteresis varied between 0.5 and 5 mA.

The size of the resistance jumps, represented by δR (the difference between no excitation and droplet excitation), were found to be field dependent, as can be seen by the increasing field, and, thus, by the increasing the polarizer magnetization angle. The measured maximum magnetoresistance is $\delta R = R / R_P \approx 0.08\%$ for fields above the saturation of the FL magnetization ($\approx$1 T), and smaller than the maximum total change of R_0 = 0.2% for the antiparallel configuration (being only $R / R_0 \approx 1/3$). Thus, the authors [128] conclude, that the spins are not fully reversed during the measurement, which is a time-average measurement of the NC resistance. One hypothesis is, that the magnetization of the FL precesses, on average, at an angle of about 70° in the NC region. Another possibility is, that the excitation is smaller than the NC size, or that the excitation moves beneath the NC during the measurement time (drift instabilities [80]).

In another work [126], results similar to that of [79] were described: the NC–STNO resistance and microwave signal generation were measured simultaneously as functions of the drive current and applied perpendicular magnetic field. Both experiments exhibited a dramatic transitions at a current-dependent critical field value. In this transition the microwave frequency was dropped 10 GHz, modulation sidebands appeared, and the resistance exhibited a jump, while the magnetoresistance sign was changed.

The behavior of the same NC device in moderate-to-high fields is shown in Fig. 14. At a critical field of $\mu_0 H_{\text{droplet}}$ = 0.65 T, five distinct transitional phenomena can be observed: (i) precession frequency exhibits a dramatic 10 GHz drop from about 30 GHz to 20 GHz, (ii) integrated microwave power (P) increases 40 times from 5 pW to a maximum of about 200 pW, (iii) device resistance exhibits a jump, (iv) magnetoresistance changes sign, and (v) modulation sidebands appear around the main precession frequency. All the five above mentioned features are clear signatures of the nucleation of a magnetic droplet soliton. The sharp drop in frequency is related to the soliton

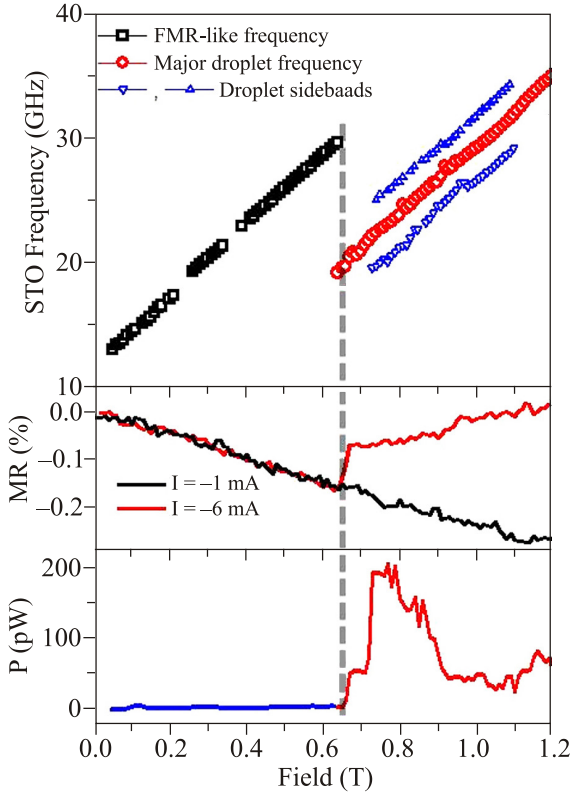

Fig. 14. (Color online) Frequency, integrated power P, and magnetoresistance MR as a function of perpendicular magnetic field at a constant current of – 6 mA through an OrthoNC–STO with 63 nm NC diameter. Below a droplet nucleation field of about $\mu_0 H_{\text{droplet}}$ = 0.65 T, the ordinary FMR-like signal is observed, increasing linearly with a 28.7 GHz/T slope. The dc MR shows a linear decrease of –0.25%/T. At $\mu_0 H_{\text{droplet}}$ the frequency drops by about 10 GHz and modulation sidebands appear. MR experiences a simultaneous jump by 0.1% and its field dependence changes sign to a positive linear slope of 0.17%/T. The integrated power jumps from 5 pW to 200 pW in two steps. From [126].

finding a balance the between exchange, anisotropy, STT, and the non-linear damping. As explained in detail in [132], a conservative (zero linear damping) magnetic droplet can, in principle, have any frequency between the FMR frequency and that given by replacing the effective field with only the applied field (called the Zeeman frequency in [132]).

The $\sim$ 33% reduction in the excitation frequency can be seen in Fig. 14. From the magnitude of the frequency drop, one can predict that the experimentally observed droplet should have a partially reversed core. The sharp increase in the generated integrated microwave power, of as much as 40 times, as observed in [126], provides a further strong indication that a droplet has been formed.

If the core of the droplet is, indeed, partially reversed, a large fraction of the droplet will have precession angles close to the equator, and, hence, make much better use of the available giant magnetoresistance of the material stack. The jump in resistance indicates that the magnetic state has changed into a more antiparallel orientation. As shown in

the inset of Fig. 14, the resistance of the device, first, decreases linearly with field, as expected for a slow out-of-plane tilting of the Co fixed layer. Without the reversal, the MR would still be negative, albeit with a weaker slope. The sign change, and the significant positive MR above the critical field, points to a substantially reversed droplet core.

Finally, the observation of the appearance of equidistant side bands can not be easily explained by the droplet nucleation alone. The sidebands indicate that an additional dynamic phenomenon modulates the original precession frequency. Micromagnetic simulations in [126] show, that one such possible phenomenon might be related to the, so-called, drift instability [132] where, under certain conditions, the droplet can escape the NC, and, as it leaves the region of the strong STT, it, eventually, succumbs to high non-linear and linear damping. By modifying the simulation parameters, it is possible to realize a situation where the droplet never leaves the NC region but instead carries out a periodic translational movement.

In the paper [123] by P. Wills and co-authors it was shown that an environment with a large NC radius, low field, modest current, and large anisotropy is less susceptible to drift, and, thus, leads to a much narrower generation linewidth of the excited magnetic droplet. Also, in this paper the conditions for the droplet existence were investigated and the state diagram was calculated (Fig. 15). The left (red) area corresponds to the condition $\sigma < \sigma_{min}$, where the droplet cannot exist. This approximately linear relation for the droplet existence boundary has been proved by experiment [129]. Also, there is the right region (blue area) where the velocity of the droplet increases until it drifts away from the NC area, and damping destroys it. The remaining white area represents the parameter space where the droplet exists, and is stable. It was also observed, that such a region shifts to lower applied fields and increased current for smaller NC radii (dashed lines).

The conditions of the droplet stability obtained in [85] were further studied in [123], and the following stability condition was obtained:

$$\alpha\omega(2\omega + h_0) > \frac{1}{2}\left[\tanh\left(\rho - \frac{1}{\omega}\right)\right], \qquad (4)$$

where ω is the precessional frequency, ρ is the dimensionless NC radius, α is the damping constant, h_0 is the perpendicular external field, and σ is the dimensionless current.

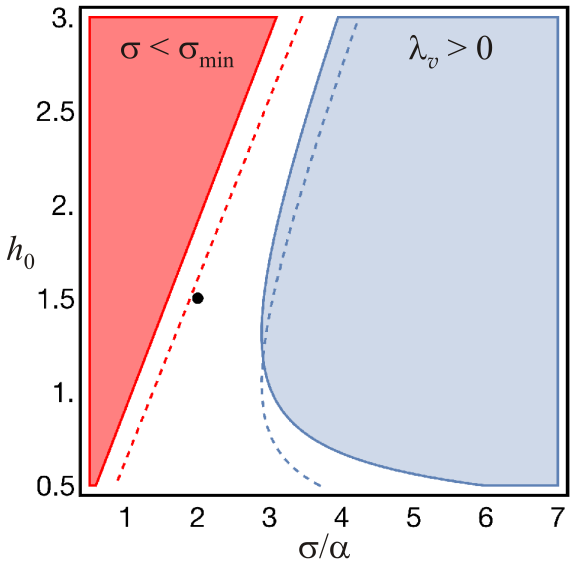

Fig. 15. (Color online) Droplet existence and linearly stable parameter space for a droplet nucleated in a NC of normalized radius $\rho = 15$. The droplet cannot exist in the left region (filled red) where $\sigma < \sigma_{min}$, whereas the droplet is linearly unstable in the right region (filled blue). The border for white/blue region is given by (4). Therefore, the droplet is stable in the remaining white region. The numerical simulations were provided for with $h_0 = 1.5$, $\alpha = 0.03$, and $\sigma = 2\alpha$ (black circle) and exhibited linear stability. The dashed lines are boundaries for droplet existence and linear stability with reduced NC radius $\rho = 5$. From [123].

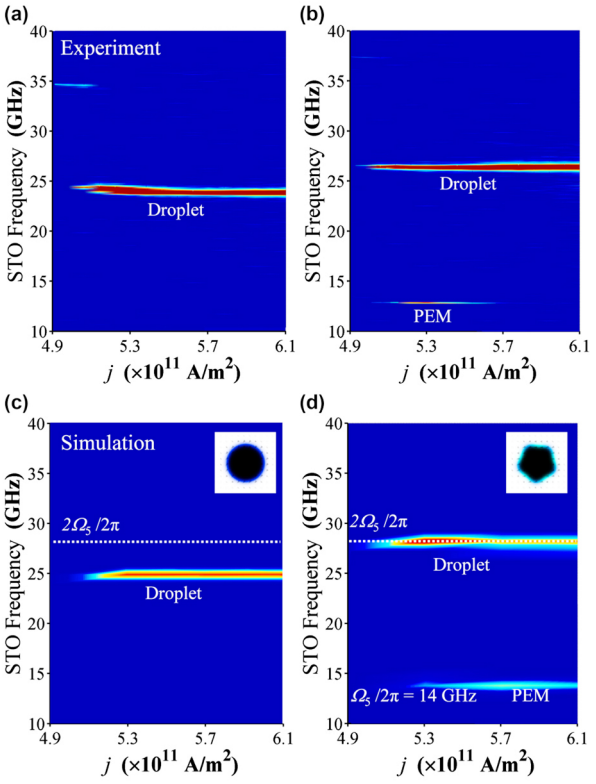

Fig. 16. (Color online) Comparison of micromagnetic simulations with experimental data on droplet PEM. Experimentally measured phase diagram of NC–STO on Co/Cu/Co-$[Ni/Co]_{\times 4}$ orthogonal spin valve with an applied magnetic field of (a) 0.8 and (b) 0.9 T with a tilt angle of 7.5°. Simulated phase diagram of the same device with slightly different field strengths and tilt angle as compared to the experimental data: (c) $H = 0.7$ T, (d) $H = 0.8$ T at a tilt angle of 3°. Other material parameters used in the simulation include R_c = 60 nm, A_{ex} = 30 pJ/m, K = 447 kJ/m^3, and M_s = = 716 kA/m. From [127].

The authors of [123] state, that the inequality requirement for the droplet stability (4) was not identified previously in [85], although it is essential for the understanding of the droplet dynamics [123].

In the paper [127] it was demonstrated, that at a sufficiently large driving currents and for a spin polarization direction tilted away from the NC plane normal, the circular droplet soliton can become unstable against the excitations in the form of periodic deformations of its perimeter. Also, it was shown in [127], that the perimeter excitation modes (PEMs) can be excited parametrically, when the fundamental precession frequency of the droplet soliton is close to the double frequency of one of the PEMs. The results of experiments [127] are presented in Figs. 16(a) and 16(b), while the results of the corresponding numerical simulations are presented in Figs. 16(c) and 16(d). These figures show the experimental and numerically calculated microwave power of a NC–STNO based on a Co/Cu/Co-$[Ni/Co]_{\times 4}$ orthogonal spin valve obtained at different applied magnetic field strengths and tilt angles. In the experiment, the PEM was excited in a field of 0.9 T tilted 7,5° from the film normal. These parameters are reasonably close to the parameters used in the numerical simulations, which were performed at a bias field of 0.8 T tilted 3°, with all the other material parameters being similar to the corresponding parameters in experiments [79].

At a sufficiently large driving dc current the main auto-oscillation mode, corresponding to the formation of a magnetic droplet soliton, appears at the frequency around 24 GHz, and continues to exist at the same frequency with the further increase of the driving dc current [see Figs. 16(a) and 16(c)].

For the analytical treatment presented in [127], both damping and STT were ignored, and the perimeter dynamics was derived for a conservative magnon drop with the fundamental precession frequency ω_0 given by the following approximate expression [17,80]: $\omega_0(H) = \omega_H + \lambda_{ex}\omega_M / \rho_0\omega_H$, where $\omega_H = \gamma\mu_0 H$, $\omega_M = \gamma M_s$, H is the magnitude of the perpendicular bias magnetic field, ρ_0 is the effective radius of the drop, $\lambda_{ex} = \sqrt{A_{ex} / K}$ is the exchange length, K is the magnetic anisotropy and A_{ex} is the exchange constant.

The characteristic frequencies of PEMs obtained in [127] were: $\Omega = \gamma(2K / M_s - \mu_0 M_s)(\lambda_{ex} / \rho)$ then the PEM eigenfrequency is given by: $\Omega_n = n\sqrt{n^2 - 1}\Omega$.

In [127] is was shown that that PEMs are only excited when the droplet precession frequency is close to twice that of the PEM. This parametric process has the energy conservation law: $\omega_0(H) = 2\Omega_n$.

When, with the increase of the bias magnetic field, the frequency of the magnetic droplet soliton of 28 GHz [see $\omega_0(H)$] coincides with the double frequency of the PEM with the index $n = 5$ (equal to 14 GHz), in both experimental and numerical simulations the parametric excitation of this PEM takes place [see Figs. 16(b) and 16(d)]. With the further increase of the driving dc current in the experiment, the PEM disappears at $j > 5.65 \cdot 10^{11}$ A/m^2 [see Fig. 16(b)], while in the numerical modeling it also disappears, but at a larger magnitude of the bias current density $j > 6.3 \cdot 10^{11}$ A/m^2 [not shown in Fig. 16(d)]. The comparison of the theory and experiment presented in Fig. 16 from [127] demonstrates that theoretical model gives a full qualitative and partly quantitative description of the internal nonlinear dynamics of the self-oscillating magnetic droplet solitons.

5. Conclusions

The pioneering works of Professor A.M. Kosevich devoted to the theoretical study of magnetic solitons led to the development of new areas in modern magnetism and to the formation of modern magnonics, where specific two-dimensional magnetic solitons, the spin-wave (SW) bullets and droplets, are widely investigated and utilized for many promising applications in magnonic and spintronic systems. In this review we summarized experimental and theoretical advances in modern magnonics and spintronics involving the magnetic bullets and droplets since their prediction and initial study by A.M. Kosevich. We briefly described the theoretical models of the bullets and droplets, and considered the key experimental results in this area of modern magnetism. We presented experimental results obtained using the Brillouin light scattering technique, that undeniably proved the existence and unusual properties of the SW bullets in magnetic films and 2D confined magnetic structures. For instance, unlike quasi-one-dimensional SW envelope solitons, the two-dimensional SW bullets are destroyed in collisions with other bullets.

We also showed that the SW bullets can be self-generated, parametrically excited and phase-conjugated like conventional spin waves, while their collapse leads to the formation of narrow SW caustic beams. We have also demonstrated that SW bullets, as standing self-localized SW modes, can be excited in magnetic nanocontacts driven by a spin-polarized or pure spin current.

In this review we considered the key experiments, simulations and theoretical results involving excitation, existence, transformation and collapsing of such bullets in spin-torque nano-oscillators.

In the last part of this review we discussed the experimental results that clearly showed the nucleation (including the case of parametric auto-excitation), internal dynamics and annihilation of SW droplets in spin-torque-driven magnetic nanocontacts, and analyzed recent theoretical papers that describe the magnetic droplet properties. The reviewed theoretical, numerical and experimental results show that SW droplets have several unusual properties due to their

strongly nonlinear nature, which, we believe, makes them suitable for applications in modern spintronic signal processing systems.

Acknowledgments

This work was supported in part by the grant from the Center for NanoFerroic Devices (CNFD) and Nanoelectronics Research Initiative (NRI), by the Grants Nos. EFMA-1641989 and ECCS-1708982 from the NSF of the USA, and by the DARPA M3(I)C Grant under the Contract No. W911–17-C-0031. This work was also supported by DFG in the framework of the Transregional Collaborative Research Center (SFB/TRR) 173 "Spin+X–Spin in its collective environment" (Project B01 "Spin+Magnon: Spin excitations for information processing"), the Ministry of Education and Science of Ukraine (grants 16BF052-01 and 18BF052-01M) and by the grant from the National Academy of Sciences of Ukraine (grant 7F). The publication contains the results of studies conducted by President's of Ukraine grant for competitive projects (F 78) and is also based on the research provided by the grants F 76 and F 83 of the State Fund for Fundamental Research of Ukraine.

1. L. Landau and E. Lifshitz, *Phys. Z. Sowjetunion* **8**, 153 (1935).
2. E. Zavoisky, *J. Phys. USSR* **9**, 245 (1945).
3. J.H.E. Griffiths, *Nature* **158**, 670 (1946).
4. *Ferromagnetic Resonance. The Phenomenon of Resonant Absorption of a High-Frequency Magnetic Field in Ferromagnetic Substances*, S.V. Vonsovskii (ed.), Elsevier Ltd., Amsterdam (1966).
5. A.G. Gurevich, *Magnetic Resonance in Ferrites and Antiferromagnets*, Nauka, Moscow (1978) (in Russian).
6. A.G. Gurevich and G.A. Melkov, *Magnetization Oscillations and Waves*, CRC Press, New York (1996).
7. A.I. Akhiezer, V.G. Bar'yakhtar, and S.V. Peletminskii, *Spin Waves*, Interscience (Wiley), New York (1968).
8. V.S. L'vov, *Nonlinear Spin Waves*, Nauka, Moscow (1987) (in Russian); V.S. L'vov, *Wave Turbulence Under Parametric Excitation*, Springer-Verlag, Berlin (1994).
9. *Spin Dynamics in Confined Magnetic Structures I–III*, B. Hillebrands (ed.), Springer-Verlag, Berlin (2002), Vol. I, (2003), Vol. II, (2006), Vol. III.
10. D.D. Stancil and A. Prabhakar, *Spin Waves: Theory and Applications*, Springer-Verlag, New York (2009).
11. *Magnetism: Materials and Applications*, É. du Trémolet de Lacheisserie, D. Gignoux, and M. Schlenker (eds.), Springer-Verlag, Boston (2005).
12. *Magnetoelectronics of Microwaves and Extremely High Frequencies in Ferrite Films*, A.A. Ignatiev (ed.), Springer-Verlag, New York (2009).
13. J. Scott Russell, in: *Rep. Fourteenth Meeting of the British Association for the Advancement of Science*, 311 (1844).
14. N.J. Zabusky and M.D. Kruskal, *Phys. Rev. Lett.* **15**, 240 (1965).
15. C.S. Gardner, J.M. Greene, M.D. Kruskal, and R.M. Miura, *Phys. Rev. Lett.* **19**, 1095 (1967).
16. V.E. Zakharov and A.B. Shabat, *Funktsional. Anal. Prilozhen.* **13**, 166 (1979).
17. B.A. Ivanov and A.M. Kosevich, *Sov. Phys. JETP* **45**, 1050 (1977).
18. A.M. Kosevich, B.A. Ivanov, and A.S. Kovalev, *Fiz. Nizk. Temp.* **3**, 906 (1977) [*Sov. J. Low Temp. Phys.* **3**, 440 (1977)].
19. A.M. Kosevich, B.A. Ivanov, and A.S. Kovalev, *Physica D* **1/2**, 363 (1981).
20. A.M. Kosevich, *Fiz. Met. Metalloved.* **53**, 420 (1982).
21. A.M. Kosevich, B.A. Ivanov, and A.S. Kovalev, *Sov. Sci. Rev. Sect. A* **6**, 161 (1985).
22. A.M. Kosevich, B.A. Ivanov, and A.S. Kovalev, *Phys. Rep.* **194**, 117 (1990).
23. A.M. Kosevich, B.A. Ivanov, and A.S. Kovalev, in: *Nonlinear Waves*, Nauka, Moscow (1979), p. 45 (in Russian).
24. A.M. Kosevich, B.A. Ivanov, and A.S. Kovalev, *Nonlinear Waves of Magnetization. Dynamical and Topological Solitons*, Naukova dumka, Kiev (1983) (in Russian).
25. A.M. Kosevich, in: *Solitons*, S.E. Trullinger, V.E. Zakharov, and V.L. Pokrovsky (eds.), Elsevier, Amsterdam (1986), p. 555.
26. A. Slavin and V. Tiberkevich, *IEEE Trans. Magn.* **45**, 1875 (2009).
27. A.N. Slavin, B.A. Kalinikos, and N.G. Kovshikov, in: *Nonlinear Phenomena and Chaos in Magnetic Materials*, P.E. Wigen (ed.), World Scientific, Singapore (1994), Ch. 9.
28. N.N. Akhmediev and A. Ankiewicz, *Solitons, Nonlinear Pulses and Beams*, Chapman and Hall, London (1997).
29. A. Slavin and V. Tiberkevich, *Phys. Rev. Lett.* **95**, 237201 (2005).
30. C. Boone, J.A. Katine, J.R. Childress, J. Zhu, X. Cheng, and I.N. Krivorotov, *Phys. Rev. B* **79**, 140404 (2009).
31. F. Sanches, V. Tiberkevich, K.Y. Guslienko, J. Sinha, M. Hayashi, O. Prokopenko, and A.N. Slavin, *Phys. Rev. B* **89**, 140410 (2014).
32. E. Grimaldi, A. Dussaux, P. Bortolotti, J. Grollier, G. Pillet, A. Fukushima, H. Kubota, K. Yakushiji, S. Yuasa, and V. Cros, *Phys. Rev. B* **89**, 104404 (2014).
33. S. Bonetti, V. Tiberkevich, G. Consolo, G. Finocchio, P. Muduli, F. Mancoff, A. Slavin, and J. Åkerman, *Phys. Rev. Lett.* **105**, 217204 (2010).
34. V.E. Demidov, S. Urazhdin, and S.O. Demokritov, *Nat. Mater.* **9**, 984 (2010).
35. O. Prokopenko, G. Melkov, E. Bankowski, T. Meitzler, V. Tiberkevich, and A. Slavin, *Appl. Phys. Lett.* **99**, 032507 (2011).
36. S. Bonetti, V. Puliafito, G. Consolo, V.S. Tiberkevich, A.N. Slavin, and J. Åkerman, *Phys. Rev. B* **85**, 174427 (2012).
37. O.V. Prokopenko, I.N. Krivorotov, E. Bankowski, T. Meitzler, S. Jaroch, V.S. Tiberkevich, and A.N. Slavin, *J. Appl. Phys.* **111**, 123904 (2012).
38. O.V. Prokopenko, I.N. Krivorotov, E.N. Bankowski, T.J. Meitzler, V.S. Tiberkevich, and A.N. Slavin, *J. Appl. Phys.* **114**, 173904 (2013).

39. O.V. Prokopenko, I.N. Krivorotov, T.J. Meitzler, E. Bankowski, V.S. Tiberkevich, and A.N. Slavin, in: *Magnonics: From Fundamentals to Applications. Topics in Applied Physics*, Springer-Verlag, Berlin (2013), Ch. 11, Vol. 125, p. 143.
40. V.S. Tiberkevich, R.S. Khymyn, H.X. Tang, and A.N. Slavin, *Sci. Rep.* **4**, 3873 (2014).
41. L. Yang, R. Verba, V. Tiberkevich, T. Schneider, A. Smith, Z. Duan, B. Youngblood, K. Lenz, J. Lindner, A.N. Slavin, and I.N. Krivorotov, *Sci. Rep.* **5**, 16942 (2015).
42. O.V. Prokopenko, *Ukr. J. Phys.* **60**, 104 (2015).
43. O.V. Prokopenko and A.N. Slavin, *Fiz. Nizk. Temp.* **41**, 457 (2015) [*Low Temp. Phys.* **41**, 353 (2015)].
44. A. Houshang E. Iacocca, P. Dürrenfeld1, S.R. Sani, J. Åkerman, and R.K. Dumas, *Nat. Nanotechnol.* **11**, 280 (2016).
45. O.R. Sulymenko and O.V. Prokopenko, in: *Nanophysics, Nanomaterials, Interface Studies, and Applications. Springer Proceedings in Physics*, Berlin: Springer-Verlag (2017), Ch. 12, Vol. 195, p. 157; O.R. Sulymenko and O.V. Prokopenko, *J. Phys. Studies* **21**, 4801 (2017).
46. A.A. Awad, P. Dürrenfeld, A. Houshang, M. Dvornik, E. Iacocca, R.K. Dumas, and J. Åkerman, *Nature Phys.* **13**, 292 (2017).
47. J.C. Slonczewski, *J. Magn. Magn. Mater.* **159**, L1 (1996).
48. L. Berger, *Phys. Rev. B* **54**, 9353 (1996).
49. M.J. Lighthill, *IMA J. Appl. Math.* **1**, 269 (1965).
50. V.P. Lukomski, *Ukr. Fiz. Zh.* **23**, 134 (1978).
51. B.A. Kalinikos, N.G. Kovshikov, and A.N. Slavin, *JETP Lett.* **38**, 413 (1983).
52. A.K. Zvezdin and A.F. Popkov, *Sov. Phys. JETP* **57**, 350 (1983).
53. A.A. Serga, A.V. Chumak, and B. Hillebrands, *J. Phys. D* **43**, 264002 (2010).
54. B.A. Kalinikos, N.G. Kovshikov, and A.N. Slavin, *Sov. Phys. JETP* **67**, 303 (1988).
55. B.A. Kalinikos, N.G. Kovshikov, and A.N. Slavin, *Phys. Rev. B* **42**, 8658 (1990).
56. B.A. Kalinikos, N.G. Kovshikov, and A.N. Slavin, *IEEE Trans. Magn.* **26**, 1477 (1990).
57. B.A. Kalinikos, N.G. Kovshikov, and A.N. Slavin, *IEEE Trans. Magn.* **28**, 3207 (1992).
58. M. Chen, M.A. Tsankov, J.M. Nash, and C.E. Patton, *Phys. Rev. B* **49**, 12773 (1994).
59. B.A. Kalinikos, N.G. Kovshikov, and A.N. Slavin, *J. Appl. Phys.* **67**, 5633 (1990).
60. A.N. Slavin, and I.V. Rojdestvenski, *IEEE Trans. Magn.* **30**, 37 (1994).
61. A.D. Boardman, S.A. Nikitov, K. Xie, and H. Mehta, *J. Magn. Magn. Mater.* **145**, 357 (1995).
62. A.N. Slavin, *Phys. Rev. Lett.* **77**, 4644 (1996).
63. A.N. Slavin, Y.S. Kivshar, E.A. Ostrovskaya, and H. Benner, *Phys. Rev. Lett.* **82**, 2583 (1999).
64. A.V. Bagada, G.A. Melkov, A.A. Serga, and A.N. Slavin, *Phys. Rev. Lett.* **79**, 2137 (1997).
65. A.L. Gordon, G.A. Melkov, A.A. Serga, V.S. Tiberkevich, A.V. Bagada, and A.N. Slavin, *JETP Lett.* **67**, 913 (1998).
66. B.A. Kalinikos, N.G. Kovshikov, and C.E. Patton, *Phys. Rev. Lett.* **80**, 4301 (1998).
67. M. Wu, B.A. Kalinikos, and C.E. Patton, *Phys. Rev. Lett.* **93**, 157207 (2004).
68. B.A. Kalinikos, N.G. Kovshikov, M.P. Kostylev, P. Kabos, and C.E. Patton, *JETP Lett.* **66**, 371 (1997).
69. G.A. Melkov, Yu.V. Kobljanskij, A.A. Serga, V.S. Tiberkevich, and A.N. Slavin, *J. Appl. Phys.* **89**, 6689 (2001).
70. A.B. Ustinov, N.Yu. Grigor'eva, and B.A. Kalinikos, *JETP Lett.* **88**, 31 (2008).
71. S.O. Demokritov, B. Hillebrands, and A.N. Slavin, *Phys. Rep.* **348**, 441 (2001).
72. M. Remoissenet, *Waves Called Solitons: Concepts and Experiments*, Springer-Verlag, Berlin (1999).
73. A. Slavin and V. Tiberkevich, in: *Spin Wave Confinement*, S.O. Demokritov (ed.), Pan Stanford Publishing, Singapore (2009), Ch. 6.
74. B.A. Kalinikos and A.B. Ustinov, in: *Recent Advances in Magnetic Insulators — From Spintronics to Microwave Applications*, M. Wu, A. Hoffmann, R.E. Camley, and R.L. Stamps (eds.), Elsevier, Amsterdam (2013), Ch. 7.
75. Y. Silberberg, *Opt. Lett.* **15**, 1282 (1990).
76. L. Bergé, *Phys. Rep.* **303**, 259 (1998).
77. M. Bauer, O. Büttner, S.O. Demokritov, B. Hillebrands, V. Grimalsky, Yu. Rapoport, and A.N. Slavin, *Phys. Rev. Lett.* **81**, 3769 (1998).
78. N. Akhmediev and A. Ankiewicz, *Dissipative Solitons: From Optics to Biology and Medicine*, Berlin, Springer (2008).
79. S.M. Mohseni, S.R. Sani, J. Persson, T.N. Anh Nguyen, S. Chung, Ye. Pogoryelov, P.K. Muduli, E. Iacocca, A. Eklund, R.K. Dumas, S. Bonetti, A. Deac, M.A. Hoefer, and J. Åkerman, *Science* **339**, 1295 (2013).
80. M.A. Hoefer, T.J. Silva, and M.W. Keller, *Phys. Rev. B* **82**, 054432 (2010).
81. M.A. Hoefer, M. Sommacal, and T.J. Silva, *Phys. Rev. B* **85**, 214433 (2012).
82. M.A. Hoefer and M. Sommacal, *Physica D* **241**, 890 (2012).
83. L.D. Bookman, and M.A. Hoefer, *Phys. Rev. B* **88**, 184401 (2013).
84. M.D. Maiden, L.D. Bookman, and M.A. Hoefer, *Phys. Rev. B* **89**, 180409 (2014).
85. L.D. Bookman and M.A. Hoefer, *Proc. Roy. Soc. A* **471**, 20150042 (2015).
86. J.J. Rasmussen and K. Rypdal, *Phys. Scr.* **33**, 481 (1986).
87. M.V. Goldman, K. Rypdal, and B. Hafizi, *Phys. Fluids* **23**, 945 (1980).
88. O. Büttner, M. Bauer, S.O. Demokritov, B. Hillebrands, M.P. Kostylev, B.A. Kalinikos, and A.N. Slavin, *Phys. Rev. Lett.* **82**, 4320 (1999).
89. A.N. Slavin, O. Büttner, M. Bauer, S.O. Demokritov, B. Hillebrands, M.M. Kostylev, B.A. Kalinikos, V.V. Grimalsky, and Y. Rapoport, *Chaos* **13**, 693 (2003).
90. A.A. Serga, S.O. Demokritov, B. Hillebrands, and A.N. Slavin, *Phys. Rev. Lett.* **92**, 117203 (2004).

91. A.A. Serga, B. Hillebrands, S.O. Demokritov, A.N. Slavin, P. Wierzbicki, V. Vasyuchka, O. Dzyapko, and A. Chumak, *Phys. Rev. Lett.* **94**, 167202 (2005).
92. G.A. Melkov, A.A. Serga, V.S. Tiberkevich, A.N. Oliynyk, and A.N. Slavin, *Phys. Rev. Lett.* **84**, 3438 (2000).
93. G.A. Melkov, A.A. Serga, A.N. Slavin, V.S. Tiberkevich, A.N. Oleinik, and A.V. Bagada, *JETP* **89**, 1189 (1999).
94. V.I. Vasyuchka, A.A. Serga, C.W. Sandweg, D.V. Slobodianiuk, G.A. Melkov, and B. Hillebrands, *Phys. Rev. Lett.* **111**, 187206 (2013).
95. A.A. Serga, M.P. Kostylev, and B. Hillebrands, *Phys. Rev. Lett.* **101**, 137204 (2008).
96. M.P. Kostylev, A.A. Serga, and B. Hillebrands, *Phys. Rev. Lett.* **106**, 134101 (2011).
97. V. Veerakumar and R.E. Camley, *Phys. Rev. B* **74**, 214401 (2006).
98. V.E. Demidov, S.O. Demokritov, D. Birt, B. O'Gorman, M. Tsoi, and X. Li, *Phys. Rev. B* **80**, 014429 (2009).
99. T. Schneider, A.A. Serga, A.V. Chumak, C.W. Sandweg, S. Trudel, S. Wolff, M.P. Kostylev, V.S. Tiberkevich, A.N. Slavin, and B. Hillebrands, *Phys. Rev. Lett.* **104**, 197203 (2010).
100. T. Sebastian, T. Brächer, P. Pirro, A.A. Serga, B. Hillebrands, T. Kubota, H. Naganuma, M. Oogane, and Y. Ando, *Phys. Rev. Lett.* **110**, 067201 (2013).
101. F. Heussner, A.A. Serga, T. Brächer, B. Hillebrands, and P. Pirro, *Appl. Phys. Lett.* **111**, 122401 (2017).
102. M. Tsoi, A.G.M. Jansen, J. Bass, W.-C. Chiang, M. Seck, V. Tsoi, and P. Wyder, *Phys. Rev. Lett.* **80**, 4281 (1998).
103. M. Tsoi, A.G.M. Jansen, J. Bass, W.-C. Chiang, V. Tsoi, and P. Wyder, *Nature* **406**, 46 (2000).
104. S.I. Kiselev J.C. Sankey, I.N. Krivorotov, N.C. Emley, R.J. Schoelkopf, R.A. Buhrman, and D.C. Ralph, *Nature* **425**, 380 (2003).
105. W.H. Rippard, M.R. Pufall, and T.J. Silva, *Appl. Phys. Lett.* **82**, 1260 (2003).
106. K.J. Lee, A. Deac, O. Redon, J.P. Nozières, and B. Dieny, *Nature Mater.* **3**, 877 (2004).
107. W.H. Rippard, M.R. Pufall, S. Kaka, T.J. Silva, and S.E. Russek, *Phys. Rev. B* **70**, 100406(R) (2004).
108. W.H. Rippard, M.R. Pufall, S. Kaka, S.E. Russek, and T.J. Silva, *Phys. Rev. Lett.* **92**, 027201 (2004).
109. I.N. Krivorotov, N.C. Emley, J.C. Sankey, S.I. Kiselev, D.C. Ralph, and R.A. Buhrman, *Science* **307**, 228 (2005).
110. J.C. Slonczewski, *J. Magn. Magn. Mater.* **195**, 261 (1999).
111. S.M. Rezende, F.M. de Aguiar, and A. Azevedo, *Phys. Rev. Lett.* **94**, 037202 (2005).
112. A.N. Slavin and P. Kabos, *IEEE Trans. Magn.* **41**, 1264 (2005).
113. G. Bertotti, C. Serpico, I.D. Mayergoyz, A. Magni, M. d'Aquino, and R. Bonin, *Phys. Rev. Lett.* **94**, 127206 (2005).
114. G. Consolo, B. Azzerboni, G. Gerhart, G.A. Melkov, V. Tiberkevich, and A.N. Slavin, *Phys. Rev. B* **76**, 144410 (2007).
115. G. Gerhart, E. Bankowski, G.A. Melkov, V.S. Tiberkevich, and A.N. Slavin, *Phys. Rev. B* **76**, 024437 (2007).
116. G. Consolo, B. Azzerboni, L. Lopez-Diaz, G. Gerhart, E. Bankowski, V. Tiberkevich, and A.N. Slavin, *Phys. Rev. B* **78**, 014420 (2008).
117. V. Puliafito, G. Siracusano, B. Azzerboni, and G. Finocchio, *IEEE Magn. Lett.* **5**, 3000104 (2014).
118. D. Backes, F. Maciá, S. Bonetti, R. Kukreja, H. Ohldag, and A.D. Kent, *Phys. Rev. Lett.* **115**, 127205 (2015).
119. V.E. Demidov, H. Ulrichs, S.V. Gurevich, S.O. Demokritov, V.S. Tiberkevich, A.N. Slavin, A. Zholud, and S. Urazhdin, *Nat. Commun.* **5**, 3179 (2014).
120. M.B. Jungfleisch, W. Zhang,J. Sklenar, J. Ding, W. Jiang, H. Chang, F.Y. Fradin, J.E. Pearson, J.B. Ketterson, V. Novosad, M. Wu, and A. Hoffmann, *Phys. Rev. Lett.* **116**, 057601 (2016).
121. S. Urazhdin, V.E. Demidov, R. Cao, B. Divinskiy, V. Tyberkevych, A. Slavin, A.B. Rinkevich, and S.O. Demokritov, *Appl. Phys. Lett.* **109**, 162402 (2016)
122. B. Georges, J. Grollier, M. Darques, V. Cros, C. Deranlot, B. Marcilhac, G. Faini, and A. Fert, *Phys. Rev. Lett.* **101**, 017201 (2008).
123. P. Wills, E.E. Iacocca, and H.A. Hoefer, *Phys. Rev. B* **93**, 144408 (2016).
124. D.V. Slobodianiuk, O.V. Prokopenko, and G.A. Melkov, *J. Magn. Magn. Mater.* **439** 144 (2017)
125. E. Iacocca, R.K. Dumas, L. Bookman, M. Mohseni, S. Chung, M.A. Hoefer, and J. Åkerman, *Phys. Rev. Lett.* **112**, 047201 (2014).
126. S. Chung, S.M. Mohseni, S.R. Sani, E. Iacocca, R.K. Dumas, T.N. Anh Nguyen, Ye. Pogoryelov, P.K. Muduli, A. Eklund, M. Hoefer, and J. Åkerman, *J. Appl. Phys.* **115**, 172612 (2014).
127. D. Xiao, V. Tiberkevich, Y.H. Liu, Y.W. Liu, S.M. Mohseni, S. Chung, M. Ahlberg, A.N. Slavin, J. Åkerman, and Yan Zhou, *Phys. Rev. B* **95**, 024106 (2017).
128. S. Lendínez, N. Statuto, D. Backes, A.D. Kent, and F. Macià, *Phys. Rev. B* **92**, 174426 (2015).
129. F. Macià, D. Backes, and A.D. Kent, *Nat. Nanotechnol.* **9**, 992 (2014).
130. S. Chung, S.M. Mohseni, A. Eklund, P. Dürrenfeld, M. Ranjbar, S.R. Sani, T.N. Anh Nguyen, R.K. Dumas, and J. Åkerman, *Fiz. Nizk. Temp.* **41**, 1063 (2015) [*Low Temp. Phys.* **41**, 833 (2015)].
131. S. Chung, Q.T. Le, M. Ahlberg, M. Weigand, I. Bykova, A.A. Awad, H. Mazraati, A. Houshang, S. Jiang, T.N. Nguyen, E. Goering, G. Schütz, J. Gräfe, and J. Åkerman, *arXiv:1707.01595* cond-mat.mes-hall.
132. M.A. Hoefer, T.J. Silva, and M.D. Stiles, *Phys. Rev. B* **77**, 144401 (2008).